PHYSICAL REVIEW VOLUME 75, NUMBER 1 JANUARY 1, 1949

# Magnetic Domain Patterns on Single Crystals of Silicon Iron

H. J. WILLIAMS, R. M. BOZORTH, AND W. SHOCKLEY
*Bell Telephone Laboratories, Murray Hill, New Jersey*
(Received August 30, 1948)

Magnetic powder patterns have been obtained on electrolytically polished surfaces of single crystals of iron containing 3.8 weight percent silicon. Domains are easily visible, outlined by accumulations of colloidal magnetic particles. Several techniques have been developed that enable the direction of magnetization in each domain to be determined. Many types of domain patterns are observed, depending on the orientation of the surface with respect to the crystal axes. The simpler patterns can now be interpreted in some detail, and support the idea that the internal domain structure is relatively simple and is usually composed of a series of plates or slabs magnetized at 45° or 90° to the plate length. In one case it is verified that the plate thickness depends on plate length in approximate accordance with theory; and, for the more complicated "tree" patterns, comparison of theory with experiment shows that good agreement can be obtained using theoretical values of the wall energy. Further verification of the theory of Bloch walls is obtained by determining from experiment the change in spin orientation on traversing the wall.

## INTRODUCTION

ALTHOUGH the domain theory of ferromagnetism has been found to be adequate in many respects, many details of domain structure, in particular the geometrical forms of the domains and their change with magnetization, have been lacking. It is generally recognized that the domains in an unmagnetized material are small regions, each saturated in a direction determined by the crystal axes or the local stresses. The change in magnetization, caused by the application of a magnetic field, takes place by movement of the boundaries between domains (in weak fields) or by rotation of the direction of magnetization (in strong fields). However, the shapes of the domains, and the ways in which the boundaries form and move with field and stress, have not heretofore been established experimentally.

In attempts to obtain visual evidence of domain structure, von Hámos and Thiessen[1] and Bitter[2] proposed independently that fine magnetic particles be spread over the surface of material to be investigated, in the hope that the inhomogeneities in the magnetization would be seen under the microscope in the same way that cracks and flaws in large pieces of iron have been detected for many years by sprinkling relatively coarse powder over the surface of the magnetized piece. This technique was developed by a number of investigators, and a considerable advance in knowledge and technique was made by Elmore and McKeehan[3] who applied a colloidal suspension of iron oxide to carefully polished specimens and observed the so-called "maze" patterns (see Fig. 2) in *unmagnetized* specimens of iron.

Later, Elmore[4] showed that the maze pattern is characteristic of the polished surface and not of the interior. He then removed the effects of mechanical polishing by electrolytic means and observed patterns on crystals magnetized at right angles to the surface. In our work we have used Elmore's method of electrolytic polishing and observed patterns on many crystal surfaces when the specimen is demagnetized and when it is magnetized to various extents parallel to the surface.

The basic theory of domains has been developed and extended by many writers. It is commonly assumed that in zero and low fields the magnetization in each domain is parallel to one or another of the directions of easy magnetization in the crystal (⟨100⟩ directions in iron). Recent progress in domain theory, particularly in domain geometry, has been made by Néel[5] using the assumption that there is a minimum number of magnetic poles at external and internal domain boundaries; this requires that the normal component of magnetization is

[1] L. v. Hámos and P. A. Thiessen, Zeits. f. Physik **71**, 442 (1931).
[2] F. Bitter, Phys. Rev. **38**, 1903 (1931).
[3] W. C. Elmore and L. W. McKeehan, Trans. A. I. Min. Met. Engrs. **120**, 236 (1936).
[4] W. C. Elmore, Phys. Rev. **51**, 982 (1937) and **53**, 757 (1938).
[5] L. Néel, J. de phys. [8] **5**, 241 (1944).

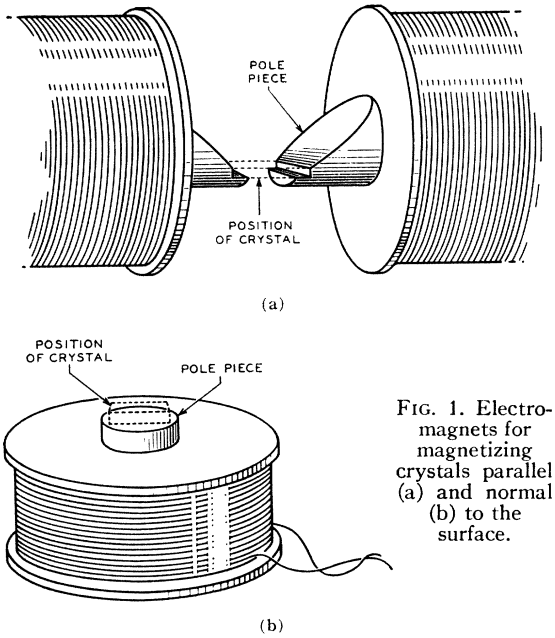


FIG. 1. Electromagnets for magnetizing crystals parallel (a) and normal (b) to the surface.

approximately constant across a boundary or "wall." The domain patterns described below are found to conform well to this principle of "flux closure" and, consequently, they represent configurations of low magnetostatic energy. The Bloch walls or transition regions which separate the domains also have energies of the order of 1 erg/cm$^2$; the stable arrangement of domains is the one which minimizes all the energies of which those of poles and domain walls are important.

In our work, the patterns on crystals of some orientations are simple and lead to definite conclusions regarding the domain structure of the whole crystal; with others they are very complex and little progress has been made in understanding them. In several instances the results confirm in a striking way the recent theoretical work of Néel.

## EXPERIMENTAL PROCEDURE

Single crystals of iron containing 3.8 weight percent silicon were prepared by melting pure materials in pure hydrogen and solidifying very slowly, as previously described.[6] Specimens were cut with surfaces approximately parallel to (100), (110), or (111) planes. They were then deeply etched and annealed, some of them at 1300°C in pure hydrogen, and carefully polished using conventional metallographic technique.

The surfaces to be examined were electrolytically polished. This operation was carried out in a bath composed of 100 g of solid chromic acid and 900 g of an 85 percent solution of phosphoric acid. The bath was heated to 90°C and electrolyzed with the specimen as anode and a copper rod as cathode, with a current of 10 to 20 amperes. A specimen having an area of 1 or 2 cm$^2$ was immersed for about one minute, or until microscopic examination showed that all scratches were removed.

The colloidal suspension was made according to Elmore's directions:[7] 2 g of hydrated ferrous chloride ($FeCl_2 \cdot 4H_2O$) and 5.4 g of hydrated ferric chloride ($FeCl_3 \cdot 6H_2O$) were dissolved in 300 cm$^3$ of hot water, and a solution of 5 g of sodium hydroxide added to it with constant stirring; this was filtered, and the precipitate of $Fe_3O_4$ washed and added to one liter of 0.5 percent soap solution, and the whole boiled for a short time. A more concentrated colloidal suspension was also made by adding the precipitate of $Fe_3O_4$ to 100 cm$^3$ of soap solution.

Powder patterns were formed by placing a drop of the colloidal suspension on the crystal surface, then placing a thin microscope cover glass on the drop so that a thin layer of the colloidal suspension was left between the crystal and the cover glass. They were usually observed under the microscope with a magnification of

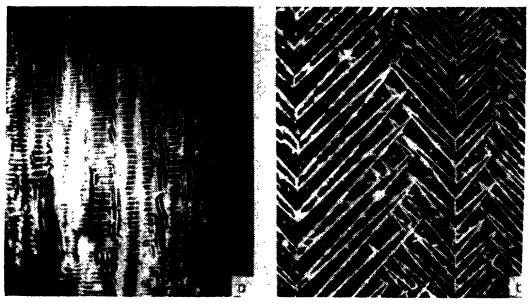


FIG. 2. Powder patterns obtained after mechanical polishing (a) and after electrolytic polishing (b) of the same surface area.

[6] H. J. Williams, Phys. Rev. **52**, 747 (1937).

[7] W. C. Elmore, Phys. Rev. **54**, 1092 (1938) and **62**, 486 (1942).

330 diameters. Ultropak dark field vertical illumination was used. Photographs were made with a Zeiss Ikon camera and Kodak Super XX 520 pack film.

When the usual colloidal suspension is used, the colloidal particles commonly form into lines, the rest of the area being almost free. On surfaces of certain crystallographic orientations, however, large portions of the field are covered with particles, other smaller portions being quite free. A pattern changes with application of field or stress, provided the solution has been freshly applied; but if it has remained undisturbed for some time—perhaps 10 minutes—it becomes "frozen" and immobile, each particle adhering to the same part of the surface in spite of change in magnetization. Before this occurs, Brownian motion of some of the particles can be observed.

Magnetization of the specimen in the plane of the surface was usually accomplished with the aid of the electromagnet sketched in Fig. 1a. Magnetization at right angles to the surface was carried out by placing the specimen on top of the iron core of an electromagnet having a vertical axis, Fig. 1b.

## TECHNIQUES FOR DETERMINING DIRECTIONS OF MAGNETIZATION IN DOMAINS

A relatively simple pattern, and one having several features that we have been able to interpret, is formed on a surface almost parallel to the crystallographic planes (100). After the specimen has been polished mechanically, using conventional metallographic technique, but not yet polished electrolytically, the usual maze pattern of Fig. 2a, reported first by McKeehan and Elmore,[8] is obtained. After electrolytic polishing of the same area the pattern of Fig. 2b is observed, and repeated treatments do not change its character. The pattern resembles the outline of a tree with the branches pointing in two of the four directions that lie in the plane of the surface and are inclined 45° to the crystal axes. A similar "tree" pattern, but less well defined, was obtained on a surface prepared with a special wax-lap technique to be described in a forthcoming article by E. E. Thomas, of the Bell Telephone Laboratories.

[8] L. W McKeehan and W. C. Elmore, Phys. Rev 46, 226 (1934).

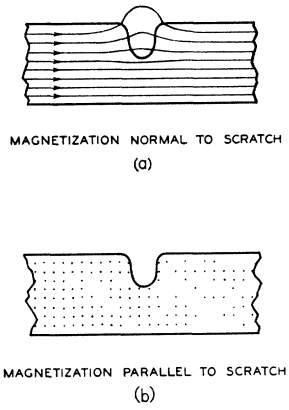


FIG. 3. (a) Illustrates how flux emerges from the metal while crossing a scratch which is normal to the magnetization in a domain; (b) shows that no flux emerges from the metal when the scratch is parallel to the magnetization in a domain.

It may be concluded that conventional mechanical polishing produces surface strains that affect the powder patterns, which cannot then be used to interpret domain structure in the interior. On the contrary, patterns on electrolytically polished surfaces are useful in obtaining information about the internal structure. This has been especially important in advancing our knowledge of domain geometry. Powder patterns can often be used to detect small surface strains.

The directions of magnetization in the various domains shown in the tree pattern have been determined by a technique involving (1) scratching the surface, and have been confirmed by (2) experiments on the effect of mechanical stress, and by (3) observation of peculiarities in the pattern obtained with the use of heavy colloid. The techniques which establish the nature of the magnetization pattern are described in the following sections, after which the theoretical explanation of the pattern is given.

### Scratch Technique

If a scratch crosses a domain in which the magnetization is not parallel to the scratch, magnetic poles are formed when the flux emerges into the air where it crosses the scratch (Fig. 3a) and colloidal particles are attracted and enhance the visibility of the scratch. If the scratch is parallel to the magnetization, no disturbance of the flux occurs (Fig. 3b) and the scratch is almost or quite invisible. In practice it was found that the

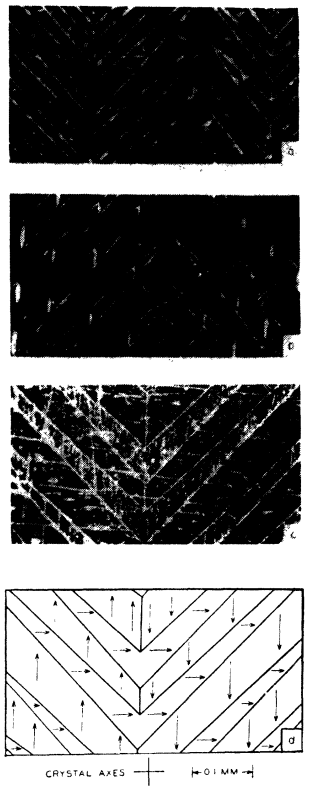


FIG. 4. (a) Typical "tree" pattern; (b) pattern on a surface having a series of parallel scratches made with a ruling engine; (c) pattern on a surface having vertical and horizontal scratches made with a brush of fine glass fibers; (d) directions of magnetization in pattern (c), as determined by the scratches.

scratch must not be so deep as to strain the surrounding material. After some experimenting, scratches were made in two ways: (i) by using a ruling engine with a conical sapphire stylus, the weight of which was carefully balanced to make a light scratch, and then polishing electrolytically to reduce the scratch still further, and (ii) by using a small brush made of fine glass fibers and passing it lightly over the surface. Scratches were always made approximately parallel to the known directions of easy magnetization, the [100] directions parallel to the sides of the figure. The results of the experiment are shown in Fig. 4. Here the first pattern is of the tree type and contains no scratches. The second was formed after vertical scratches had been made with a ruling engine. The third pattern shows two mutually perpendicular sets of scratches made with a brush having fine glass fibers, and the fourth part of the figure is a diagram showing the domain boundaries and directions of magnetization in the third pattern, deduced from the behavior of the colloid around the scratches. In the diagram the sense of the magnetization vector is chosen so that there is almost no change in the normal component of magnetization across a boundary, a condition*,[9,10] equivalent to the practical absence of magnetic poles at the boundary, and one which can be applied consistently throughout the whole pattern.

### Striations of Colloid

It will be noted on many of the patterns (e.g., Figs. 6 and 10a) that between the domain boundaries there are irregular elongated masses or striations of colloidal particles which are larger and more numerous when the colloidal suspension is more concentrated. Such striations were observed repeatedly to be elongated in a direction at right angles to the direction of magnetization, as determined independently by other means, and so came themselves to be reliable indicators of direction of magnetization.

The reason for the orientation of the striations is not known with certainty, but a possible

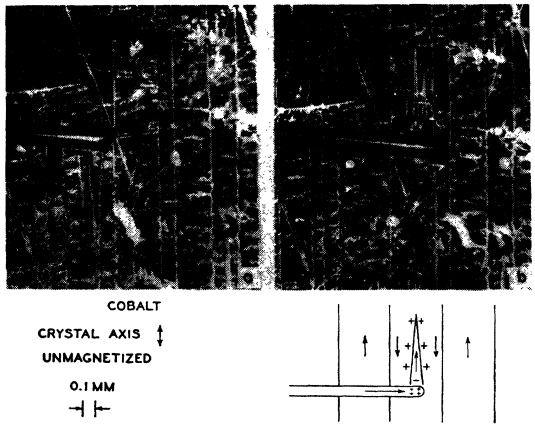


FIG. 5. Powder pattern showing regions of reversed magnetization induced by a permanent magnet probe, (a) before and (b) after moving the probe to the right so that it is above the adjacent domain. In (b) the regions of reversed magnetization are above the probe, in (a) they are below.

* The importance of this condition has been mentioned by Landau and Lifshitz (reference 9) and others, cf. references 7 and 10.

[9] L. Landau and E. Lifshitz, Physik Zeits. Sowjetunion **8**, 153 (1935).

[10] L. Néel, J. de Phys. [8], **5**, 241 (1944).

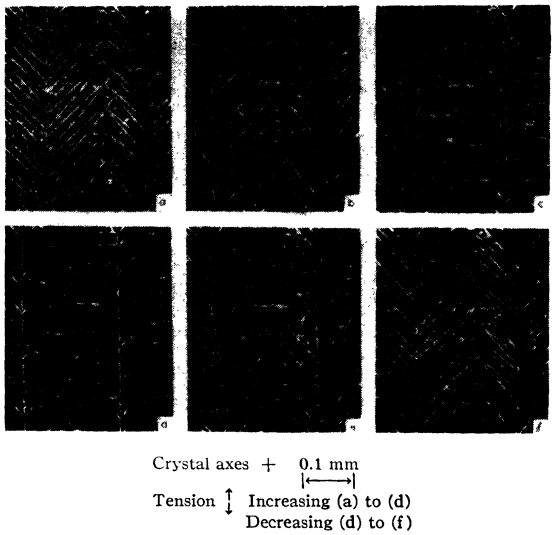


FIG. 6. (a) to (d), patterns all observed on the same area of a crystal, with tension increasing from zero to a maximum value. In (d) to (f) tension is decreasing from maximum value to zero.

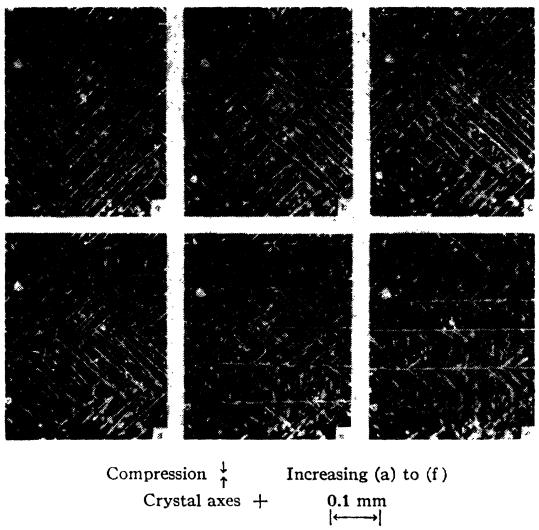


FIG. 7. Series of patterns, all observed on the same area of a crystal, as the compression was increased from zero to a maximum value.

explanation is as follows. The surface is not perfectly plane but has some irregularities that may be represented, for convenience, as a series of circular mounds. When the magnetization of the domain lies in the direction of the line connecting two mound centers, there will be magnetic poles produced in the valley between the mounds and the powder will collect in this region which will be elongated at right angles to the direction of magnetization ("transverse" striation). When the line between mounds lies at right angles to the direction of magnetization, no poles will lie in the valley between them and so no "longitudinal" striations will form. It is in a somewhat similar way that the colloid collects on mechanical scratches (see above) and is always elongated at right angles to the magnetization. The mound picture is supported by microscopic observation of a surface subjected to repeated electrolytic etching—the surface finally acquires an uneven appearance not unlike that of an orange peel. It is also supported by the fact that the striations form in the same places after successive demagnetizations. Imperfections in the structure completely below the surface might have a similar effect in producing striations.

### Probe Technique

The direction and sense of the magnetization in a domain was determined with the aid of a long, thin probe consisting of a 0.015-cm wire of a permanent magnet material (Vicalloy), magnetized and placed on the surface to be examined while the colloid was present. The pole at the end of the probe produces a field in the underlying domain. If this field is in the same direction as the magnetization of the domain, this magnetization will not be affected. If it is in the opposite direction, it will cause a local reversal of magnetization within the domain, and one observes a number of pointed regions as depicted in Fig. 5a, immediately below the end of the probe. In Fig. 5b the probe has been moved to the right so that the end lies on the next domain; here it is noted that the pointed regions lie above the probe. These photographs (of cobalt) show that the domains mentioned are magnetized in antiparallel directions, and the sign of the pole on the probe (positive) proves that the first domain is magnetized toward the top and the second toward the bottom of the figure as indicated in the diagram.

### Effect of Stress

Tension was applied to the upper surface of a thin single crystal, in a device that held the ends of the crystal fixed while a screw underneath the middle of the crystal pressed upwards. A series of patterns, obtained as the tension was first increased and then decreased in successive stages,


FIG. 8. Powder pattern on a surface having the lower half accurately parallel to a (100) plane, and the upper half inclined at an angle of 3° by rotation about a horizontal axis at the intersection of the two surfaces.

are reproduced in Fig. 6. According to domain theory, tension applied to a material having positive magnetostriction will increase the volume of the domains aligned parallel to the axis of the tension and decrease the volume of those making an angle of 90° with the axis. In the figure the areas of the tapered regions or "branches" are decreased and the areas having 180° boundaries are increased. In accordance with theory and with other considerations mentioned above, it is concluded that the tapered regions are magnetized at 90° to the (vertical) axis of tension and that for the highest tension (Fig. 6d) these regions practically vanish so that the material is then composed of domains oriented in the two senses of the tension axis. Thus the directions of magnetization deduced from the tension experiment agree with those determined by means of scratches and the striations of colloid.

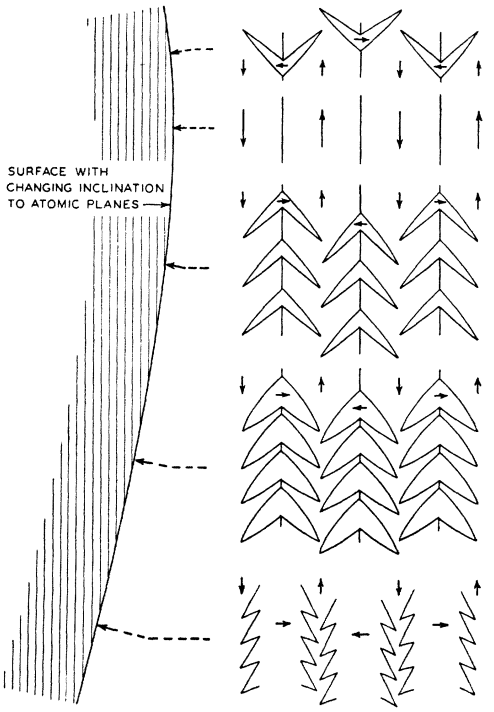


FIG. 9. Diagram showing the domains on a curved surface having a gradually varying inclination with respect to a (100) plane.

Compression was applied to the upper surface of the same specimen by clamping one end and forcing the other end upward with a screw. Results are shown in Fig. 7, with the compression axis now vertical (toward the top of the figure). One expects the pattern obtained with high elastic compression to be made of horizontal lines, 180° boundaries between domains pointing to the right and to the left. Since there are no horizontal boundaries in the pattern of the unstrained crystal in the portion of the specimen chosen for examination, these may be expected to form when a small compression is applied and to grow with increased compression until they constitute the whole pattern. These changes actually do occur, but not in a smooth way. Whole portions of the pattern change suddenly, even when the compression is increased slowly, in a way that cannot be followed by eye. With increasing compression the vertical 180° boundaries disappear, horizontal 180° boundaries form, and the 90° boundaries eventually disappear as expected (Fig. 7f).

### SURFACES SLIGHTLY INCLINED TO (100)

The conditions under which the "tree" pattern forms, and the reasons for the formation of this particular kind of pattern, are fairly well understood and will now be described.

In a preliminary experiment a specimen was selected that had rounded edges, and colloid was deposited near these edges. The tree pattern appeared only when there was a slight inclination of the surface to (100) planes, and the branches were always oriented so that they pointed at $\pm 45°$ to the "downhill" direction, the (100) planes being regarded as level.

On another specimen two plane surfaces were ground, one accurately parallel to (100) and the other inclined 3° thereto. Powder patterns were

then photographed over the ridge where the two surfaces join as shown in Fig. 8. Here again it was apparent that the tree pattern is characteristic of a surface inclined to (100) and that the branches point "down-hill."

In a more systematic experiment a curved surface was cut on a single crystal, as indicated schematically in Fig. 9. The pattern of Fig. 10(b) corresponds to the surface parallel to (100), (a) to a slope in one direction and (c) to (h) to increasing slope in the other direction. When the inclination between surface and crystal planes becomes relatively large the "branches" of the tree pattern become thick and are close together, until finally only the outlines of the end portions of the branches remain. At this stage most of the surface is magnetized transversely to the "tree trunks," and the remainder, on which most of the colloid collects, has the appearance of trees inverted from their original positions, as shown schematically in Fig. 9.

These observations can all be correlated on the basis of domain theory and, as is shown in detail in the appendix, the principal features can be understood semiquantitatively. The patterns represent minimum energy configuration in the form of a compromise between magnetostatic (pole) and domain wall energy.

Figure 11 shows the crystal surface which is tilted by an angle $\theta$ in respect to the crystal axes, $XYZ$. The underlying domains, which are magnetized parallel to [010] and [0$\bar{1}$0], produce a density of magnetic poles of $\pm I_s \sin\theta$ on the surfaces of alternating strips of width $W$. This gives rise to a magnetostatic energy, discussed in the Appendix, proportional to $W \sin^2\theta$ per unit area. When $\theta$ is larger than 1°, it is possible to reduce this energy by forming the tree patterns even though domain wall energy is added. Figures 12 and 13 show how this occurs. The branches are actually shallow domains about $\frac{1}{10}$ as thick as they are wide. They transport flux across the trunks of the trees and as they taper this flux is distributed as magnetic poles over the domain wall separating the branch from the underlying domain. The net result is to change the regions, on which there are poles, from strips of width $W$ to strips approximately as wide as the branches, and so to reduce the magnetostatic energy about tenfold for the trees of Fig. 12. It would be reduced still more if the branches were narrower; however, to use narrower branches would require more domain wall surface. Using constants based on large-scale measured properties of the material, a minimum energy theory

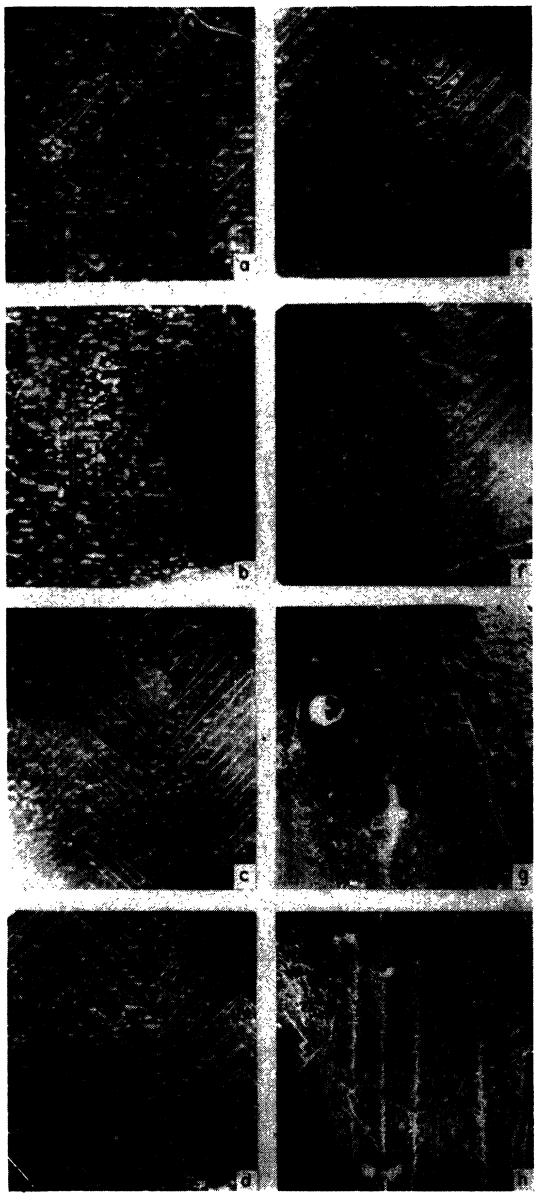


FIG. 10. Series of patterns observed at successive positions, (a) to (f), on a curved surface. Note correspondence to Fig. 9. Patterns in (g) and (h) were obtained with lower magnification, on surfaces corresponding to (b) to (d) and (d) to (f), respectively.

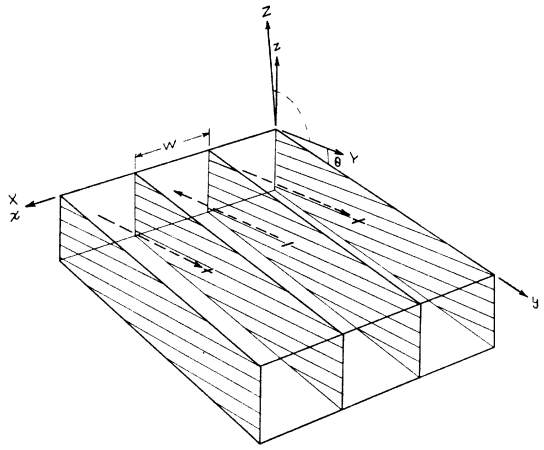


FIG. 11. Diagram showing the domain structure and distribution of poles as they would be if superficial domains ("branches") were absent.

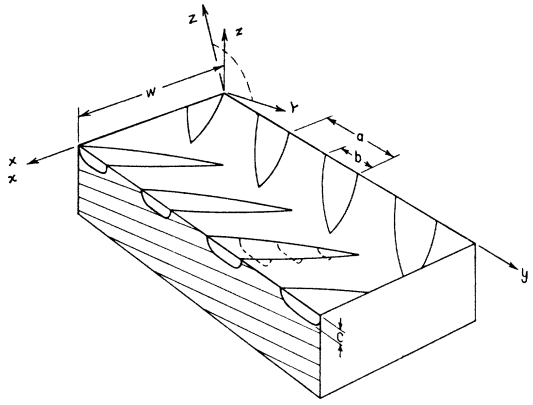


FIG. 12. Domain structure of the tree patterns.

has been worked out in the Appendix, and values for the dimensions $a$ and $b$ have been predicted. The computed values for $a$ and $b$ are about twice too large; considering the approximations involved in the theory, this may be regarded as a satisfactory confirmation of the model proposed.

The patterns at steeper slopes represent a continuous progression from the open tree patterns. From a theoretical viewpoint, however, it is simpler to regard them as modifications of the flux closure pattern of Fig. 14. In this pattern domains magnetized along [100] and [$\bar{1}$00] directions (the axes being as for Figs. 11 and 12) completely transport the flux which would otherwise emerge from the underlying domains. Figure 14a shows the arrangement of these domains with one of them removed and inverted at (b) to show its shape. It may be shown by calculation (i) that these domains can be constructed so that the geometrical pattern will be as indicated and (ii) that they do close flux correctly between [010] and [0$\bar{1}$0] domains. If the surface is tilted by $\theta$ in respect to the crystal axes, then the unit normal to the domain wall has direction cosines along $X$, $Y$, $Z$ of $\pm\sin\theta/(1+\sin^2\theta)^{\frac{1}{2}}$, $\sin\theta/(1+\sin^2\theta)^{\frac{1}{2}}$, $\cos\theta/(1+\sin^2\theta)^{\frac{1}{2}}$. The The flux closure is indicated in (c) which is a view parallel to the surface of the specimen. Theory shows that this perfectly closed pattern is less stable than that shown in (d) for which the wall energy is somewhat less but, since magnetic poles are present as shown, there is some magnetostatic energy. The quantitative theory given in the appendix shows the same degree of agreement as for the tree patterns, the computed width of $S$ which corresponds to the bright strips in Fig. 10(h) being about $\frac{1}{3}$ of the observed width. The dense deposit of colloid in Fig. 10(f) and (h) is readily understood on the basis of this model, since the pole density on the strips $S$ and, consequently, the magnetic field are proportional to $\sin\theta$.

### Effect of Vertical Field

A more direct confirmation of the pole density distribution of Fig. 13 has been obtained by

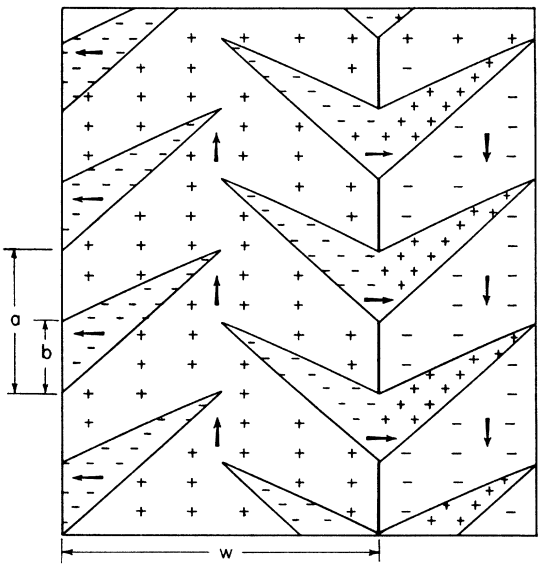


FIG. 13. Distribution of the magnetic poles on a tree pattern. Poles on branches are below surface level.

superposing a weak external vertical field (normal to the surface) which does not appreciably disturb the domain boundaries. This field adds to the underlying field in some areas and subtracts in others, depending on the sense of the underlying field, and thus gives rise to an unsymmetrical distribution of the colloid. The results of this experiment are shown in Fig. 15, and it may readily be seen that the patterns are just as predicted from the model of Figs. 12 and 13. Use of a vertical field thus permits determination of the sense of the magnetization vector in each domain.

It is to be noted that there is a very marked asymmetry in the intensity of the domain boundaries. In the next section we shall show that this is just what should be expected on the basis of the Bloch theory of the wall applied to the tree patterns.

Tree patterns of a somewhat different kind are observed on surfaces cut with the long dimension parallel to $[0\bar{1}1]$ and its surface inclined slightly to (100) in such a way that the $[0\bar{1}1]$ direction (instead of the [001] direction) lies accurately in the surface (Fig. 16). They can be interpreted satisfactorily in a way quite analogous to that just described.

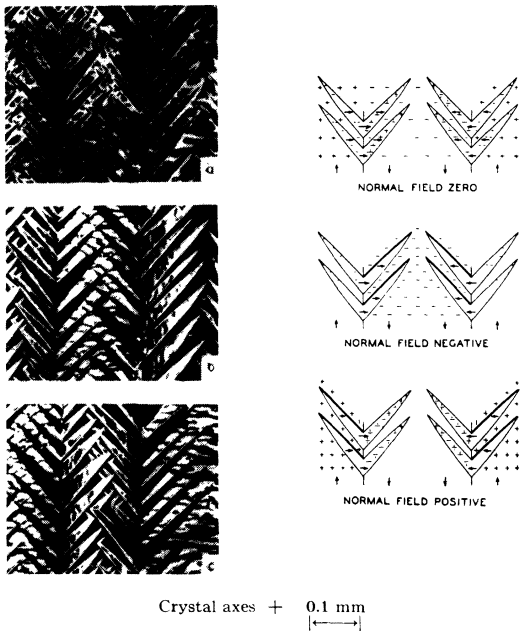


FIG. 15. Tree patterns showing the effect of applying a field of 30 Oersteds normal to the surface; (a) normal field zero, (b) normal field directed into the surface, (c) normal field directed outward from the surface.

### SPIN ORIENTATION IN THE BLOCH WALLS

We shall next show that the theory of spin orientation, together with the domain model of Fig. 12, leads to precisely the observed asymmetry in the lines of the powder pattern. This involves describing the magnetization pattern in sufficient detail to include the variations within the walls themselves. Figure 17 represents this situation; (a) shows the tree pattern and (b) an enlarged portion of (a) showing the structure of the domain wall. The directions of magnetization in the branch and in the underlying domain are indicated by the arrows in the small cubes whose

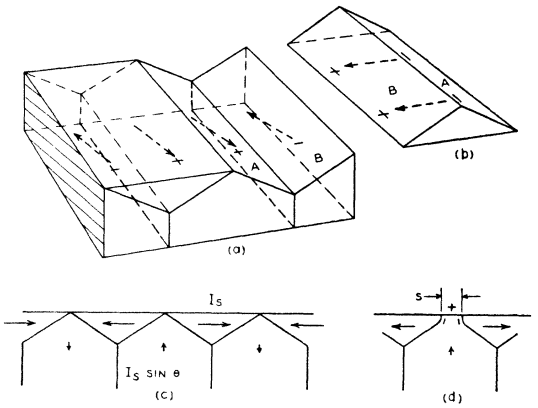


FIG. 14. (a), (b), and (c) show possible method of complete flux-closure for domain structure of Fig. 11; (d) shows structure modified to reduce wall energy and total energy.

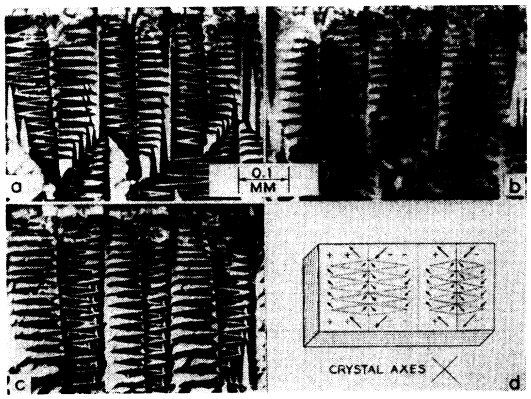


FIG. 16. Second kind of tree pattern; (a) field applied normal to the surface, (b) normal field zero, (c) normal field reversed, (d) diagram of directions of magnetization in the domains, crystal axes, and the inclination of the surface to the atomic planes (represented by lines on crystal edges).

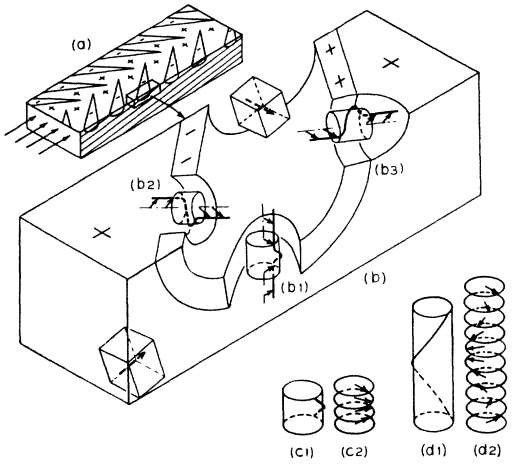


FIG. 17. The course of spin orientation during traversal of a domain wall in the tree pattern (see text).

edges are parallel to the crystal axes. The theory of domain walls requires that the component of magnetization along the normal to the wall remain substantially constant; thus attention can be concentrated on the component in the plane of the wall. The course of the spin orientation for the location (b1) is shown in (c2); here the magnetization vector is represented at the top, bottom and two intermediate points of the domain wall. The course of the component in the plane of the wall can thus be represented by a helical trace on a cylinder (c1); this convention is similarly employed in (b2) and (b3). It should be noted that this trace has the sense of a left-hand screw in all cases. This prediction is based on a consideration of the situation at (b1); if the screw were right-handed, the total angle turned through would be 270° as indicated in (d) rather than 90° as in (c). The right-hand screw would require about three times as much energy, and for that reason the left-hand screw is predicted for locations like (b1) near the bottom of the branch domain. Furthermore, if some parts of the wall have a left-handed course and others right-handed, lines of poles will be produced at boundaries between these parts and will add to the energy. Thus it is predicted that the entire wall will have a left-handed form. Within the wall itself there is a net flux from left to right in (b) which produces lines of poles where the wall strikes the surface of the specimen, and it is these lines of poles which cause the domain walls to capture colloid. The polarity of the poles, and hence the predicted course of spin orientation, can be verified by the vertical field experiments. The prediction from Fig. 17(b) can be summarized by saying that where the angle between the branch and the trunk is acute. the domain wall will have poles like those on the "sky" and where the angle is obtuse the domain wall will have poles like those on the branch. Inspection of Fig. 18 (an enlargement from Fig. 15(c)) shows that this prediction is born out in detail.** Considering that the domain wall is only about 500 to 1000A thick, it is especially gratifying that information on its internal structure can be obtained so directly.

## EFFECT OF FIELD ON (100) PATTERNS

A specimen of a single crystal, $2.3\times0.6\times0.25$ cm$^3$, with edges approximately parallel to the cubic axes, was magnetized to various degrees with the electromagnet of Fig. 1(a). The direction of magnetization, [001], lay parallel to the long edge, and its intensity was determined with the use of a search coil and ballistic galvanometer. The patterns on one of the $2.3\times0.6$ cm$^2$ faces are shown in Fig. 19. The specimen was initially demagnetized, and the field then increased in steps to a high value ((a) to (f)), then again to zero (remanence). The tree pattern observed in the demagnetized state is consistent with the

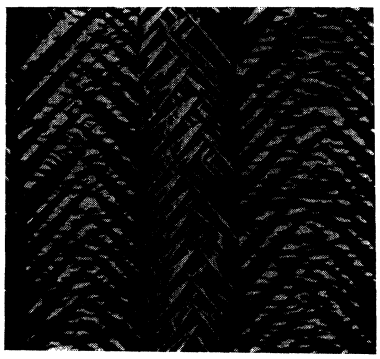


FIG. 18. Tree pattern with field applied normal to the surface, showing redistribution of colloid over the domains, intensification of some domain boundaries and disappearance of others, as compared with pattern obtained with no normal field (cf. Fig. 15).

** Except for some irregularities resulting from variations in illumination, focus, and uneven colloid distribution.

slight inclination, 1.5°, of the surface to the (100) plane.

In a preliminary experiment the specimen was demagnetized repeatedly and the pattern observed after each demagnetization. The general features of the patterns were always the same —that is, the pattern was of the tree type—but the details were never the same. In none of our experiments on electrolytically polished surfaces have we been able to reproduce a pattern of lines after a substantial change in magnetization. Careful observation shows that the lines do not tend to reform at the same place on the surface. This is in contrast to the maze patterns obtained after mechanical polishing; these can be reproduced accurately, and one concludes that they are determined by the mechanical condition of the surface, and not primarily by magnetic forces.

In Figs. 19(c) and (d) the character of the pattern is seen to be definitely different from that of (a); of the two sets of almost-parallel lines one set of lines is now predominant. When the magnetization is above 12,000 they have become so long that the whole field of view is crossed by only one set of lines.

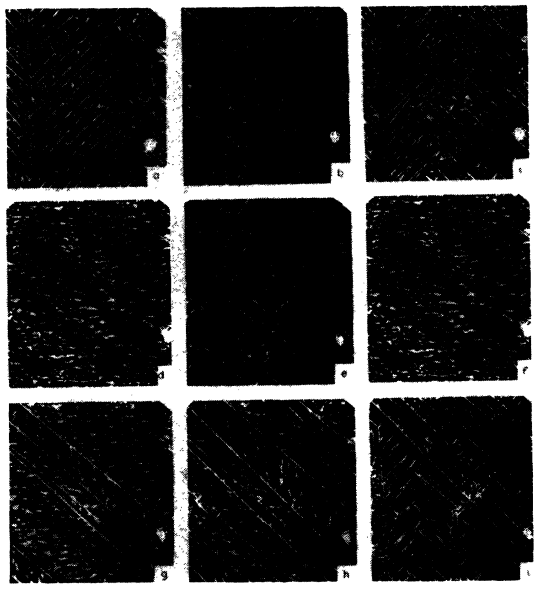


FIG. 19. Patterns on a surface inclined slightly to a (100) plane, with applied field and length of the crystal parallel to the [001] direction: (a) $B=0$, (b) $B=7000$, (c) $B=10{,}000$, (d) $B=11{,}600$, (e) $B=15{,}000$, (f) $B=18{,}600$, (g) $B=17{,}600$, (h) $B=17{,}400$, (i) $B=15{,}400$.

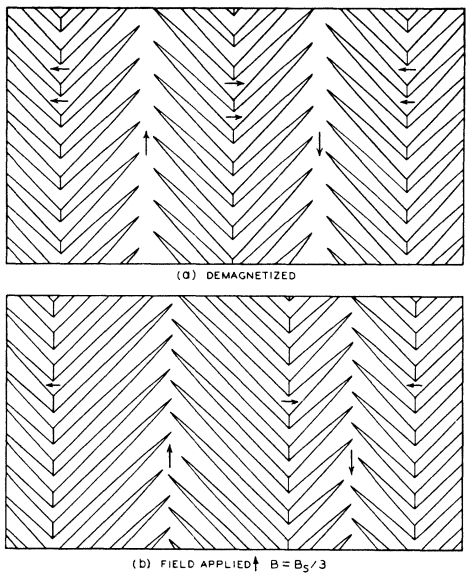


FIG. 20. Diagrams of the tree pattern showing the effect of applying a field.

Patterns of this kind were observed under lower magnification in order to be able to see a larger portion of the surface at once. It was then noticed that the whole tree pattern shifts with application of a field, the "trunks" moving sideways in one direction or the other so that the areas magnetized parallel to the field become larger and those antiparallel become smaller, and so more flux is permitted to travel in the direction of the field. This is shown schematically in Fig. 20. The "branches" of the trees extend to the middle of the domain, whatever its width, and when the specimen is magnetized the trees have branches that are usually longer on one side than on the other.

Experiments were carried out on a different specimen with the field applied parallel to a [011] direction lying in the specimen surface, a (100) plane. The patterns are reproduced in Fig. 21. When the magnetization is relatively low one notices some branch-like markings that are similar to those shown in Fig. 16 and, like them, may be attributed to a slight deviation of the surface from the (100) plane. The diagonal lines of Figs. 21(a) and (b) are 180° boundaries, similar to those shown in the pattern and diagram of Fig. 27 and referred to below in connection with

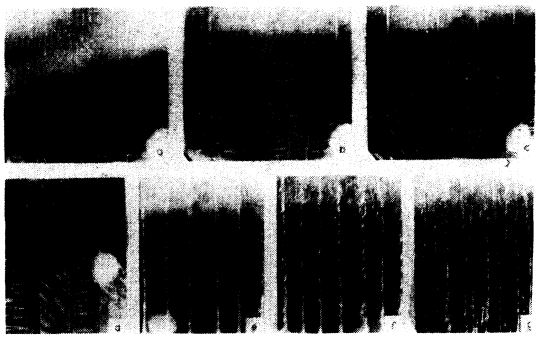


FIG. 21. Patterns on a (100) surface, with length of crystal and applied field parallel to the [011] direction. (a) $B=0$, (b) $B=9000$, (c) $B=14,500$, (d) $B=15,500$, (e) $B=15,900$, (f) $B=18,500$, (g) $B=20,000$.

that figure. Above these boundaries the magnetization goes in a zigzag manner from left to right with a component parallel to the direction of the applied field, whereas below these boundaries the net magnetization is from right to left. When the applied field is increased, the boundaries move toward the bottom of the figure (b) and finally out of the field of view (c), so that there is an increase in the areas magnetized more nearly parallel to the field at the expense of areas less favorably magnetized.

When the magnetization is relatively high ($B-H\doteqdot 16,000$) the pattern is simply a series of parallel lines, approximately equally spaced, and readily interpretable. When the field is so high (g) that the magnetization vectors are rotated out of the direction of easy magnetization and the angle between the local magnetization and the field is less than 45°, it is still true that there are no poles at domain boundaries and that the normal component of magnetization of the whole specimen is zero.

The decreasing distance between lines with increasing magnetization is in agreement with the reports of Kaya[11] and of Sixtus,[12] and with the theoretical work of Néel, as discussed below.

## PATTERNS ON (110) AND (111) SURFACES

More complicated patterns have been observed on (110) and (111) surfaces. Figure 22 shows patterns taken with increasing magnetization on a surface parallel to (110), the field being applied in the $[1\bar{1}0]$ direction in the plane of the surface. These patterns will be discussed in the next section.

Patterns obtained on surfaces parallel to (111) planes are even more complicated than those on (110) surfaces. This may be expected, since no direction of easy magnetization lies in the surface. The effect of increasing field, applied in the $[1\bar{1}0]$ direction (lying parallel to the surface) is shown in Figs. 23(a) to (f). Figure 23(g) is a second pattern of material in the unmagnetized condition; it covers an area different from that of the other patterns and is chosen to show three sets of the stronger lines, each set making an angle of 120° with the others. This corresponds to the threefold symmetry of the crystal plane. The detail of the pattern is believed to be characteristic not of the interior but only of the surface, which probably has many poles and domains of closure of the kind discussed by Landau and Lifshitz.[9] No explanation of its detailed form has been given.

It appears that internal domain structures in an unmagnetized material are generally simple,

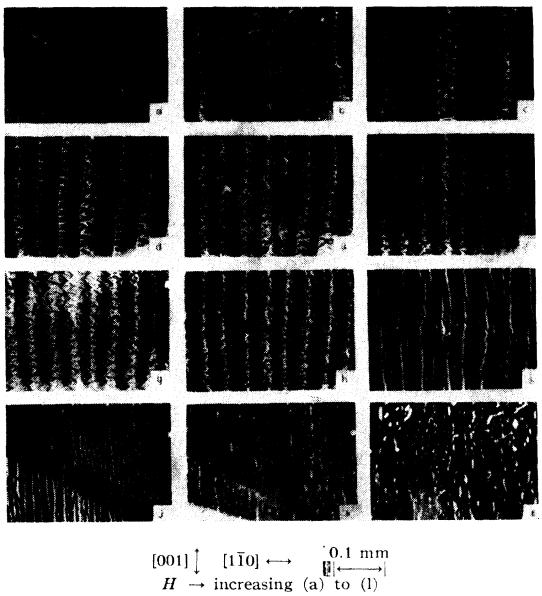


FIG. 22. Patterns on a (110) surface, with length of crystal and applied field parallel to the $[1\bar{1}0]$ direction. (a) $B=0$, (b) $B=14,800$, (c) $B=15,000$, (d) $B=15,200$, (e) $B=15,700$, (f) $B=16,400$, (g) $B=17,100$, (h) $B=18,200$, (i) $B=20,000$, (j) $B=20,200$, (k) $B=20,300$, (l) $B=20,500$.

[11] S. Kaya, Zeits. f. Physik **89**, 796 (1932) and **90**, 551 (1934).
[12] K. J. Sixtus, Phys. Rev. **51**, 870 (1937).

and that near the surface a more complicated structure is likely to occur. Domains of closure may form, or a fine-grained pattern may appear and give a distribution of poles with which a lower energy is associated. Only when a simple crystallographic plane and directions of easy magnetization are parallel to the surface has a simple structure, apparently representative of the interior, been observed.

### Relation to Néel's Theory

Following the work of Landau and Lifshitz,[9] Néel[13] has investigated theoretically the domain structure of specimens of single crystals of various geometrical forms, oriented in different ways with respect to the crystallographic axes. He considers the energies associated with domain boundaries, crystal anisotropy, and magnetization, and selects the domain structure that has the lowest energy consistent with the assumption that there are no poles at internal domain boundaries.

A comparison of his theory with our experiments can be made when the specimen is a slab having its long dimension and magnetization parallel to a $[0\bar{1}1]$ direction, its large surface parallel to a (100) plane, and its sides parallel to (011). Figure 24(a) and (b) show the orientation with respect to the crystal axes, and the theoretical domain structure near remanence (a) when all of the domains are magnetized in direc-

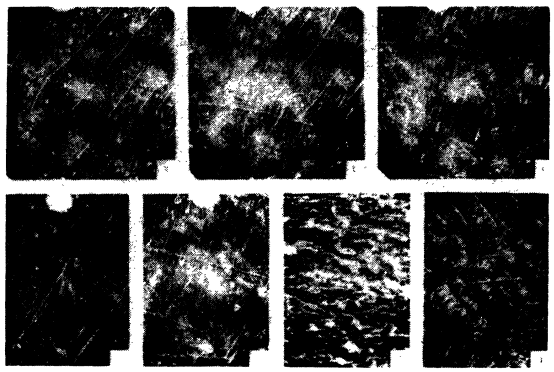


FIG. 23. Patterns on a (111) surface. (a) $B=0$, (b) $B=4000$, (c) $B=4800$, (d) $B=15{,}000$, (e) $B=15{,}500$, (f) $B=19{,}800$, (g) pattern on another area ($B=0$).

[13] L. Néel, J. de Phys. [8] 5, 265 (1944).

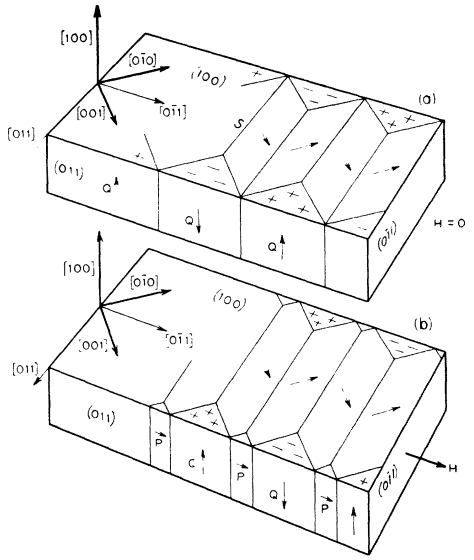


FIG. 24. Domain structure proposed by Néel; (a) without applied field, (b) with applied field.

tions making 90° or less with the direction of the applied field. The structures of (a) and (b) are composed primarily of domain sheets, $S$, oriented at right angles to the direction of the field. At the edges are domains $P$ and $Q$, having a geometry that reduces the number of poles that would be present on the surface if the domain sheets constituted the whole of the specimen. Domains $S$ and $Q$ are magnetized parallel to directions of easy magnetization. Domains $P$, on the contrary, are directed about 45° from the nearest direction of easy magnetization and consequently possess some energy of anisotropy.

The powder patterns observed on the top (100) surface of a specimen (see Fig. 21(c)), when the magnetic induction is above 14,000, correspond to the diagram of Fig. 24. The principal domain boundaries make an angle of 90°, and the directions of magnetization ±45°, to the direction of the field, and the absence of colloidal particles between lines suggests that there are no poles on this surface.

The patterns on the (011) surface (Fig. 22) also correspond in many of their features to the theoretical pattern. When the induction is less than about 15,000, the domains are magnetized at right angles to the direction of the field, and these regions may be identified with the $Q$ domains of Fig. 24. At higher inductions the

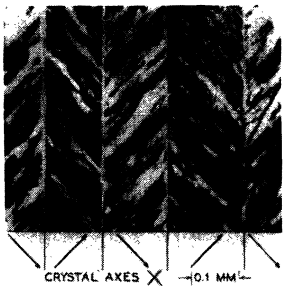


FIG. 25. Pattern obtained with a concentrated colloid on a (110) surface with striations of colloid indicating directions of magnetization (perpendicular to striations).

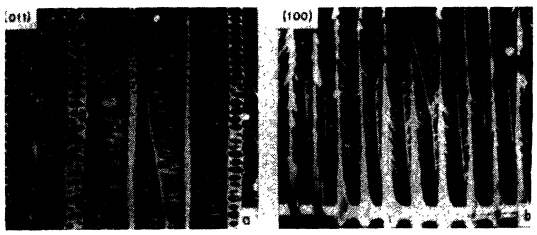


$H$ parallel to $[0\bar{1}1]$ → 0.1 mm

FIG. 26. Patterns obtained on the side and top surfaces of a crystal such as that shown by the drawing of Fig. 24: (a), (011) surface; (b), (100) surface. The lower part of the (b) pattern shows accumulations of colloid extending beyond the edge of the crystal.

boundaries seem to become wide (Fig. 22(c)), and new domains appear with complicated structure. These are the $P$ domains of Fig. 24. As the induction increases the $P$ domains grow at the expense of the $Q$ domains, and at $B = 18{,}000$ they cover practically the whole surface. This is in agreement with theory.

The fact that the $P$ domains collect colloidal particles unevenly indicates that poles are present and that the surface has a complicated domain structure. The situation is then more complex than Néel's picture suggests. Apparently the magnetization in the $P$ domains is not drawn out of the direction of easy magnetization and entirely into the $[0\bar{1}1]$ direction, but some flux penetrates the surface to form poles. These facilitate the formation of small domains of reversed magnetization,[14] and effect a complicated pattern. Also, at high inductions the domain boundaries are not straight lines but are irregular in form.

[14] E. Lifshitz, J. Phys. U.S.S.R. **8**, 337 (1944).

In order to check some of the conclusions derived from the patterns on (100) and (011) surfaces (Figs. 21 and 22), additional patterns were made with heavy colloid. Figure 25 corresponds to Fig. 21(e) in all respects except that the colloid was more concentrated, and the character of the striations of colloid confirms the previous conclusion that the directions of magnetization are inclined $\pm 45°$ to the direction of the field. Figure 26(a) corresponds to Fig. 22(c) and shows plainly that the $Q$ regions are magnetized at 90° to the direction of the field. In Fig. 26(b) the edge of the crystal is in plain view, and the collection of particles at equally spaced regions shows that the poles here are quite strong; this is in agreement with Fig. 24(b).

Figure 27 is a pattern observed with low magnification on the (100) plane with zero magnetization. It is the same as Fig. 21(a), except that a larger area is visible. It corresponds in general features to the large top surface of Fig. 24(a) by having a prominent series of parallel lines at right angles to the long dimension, and having domains of closure near the

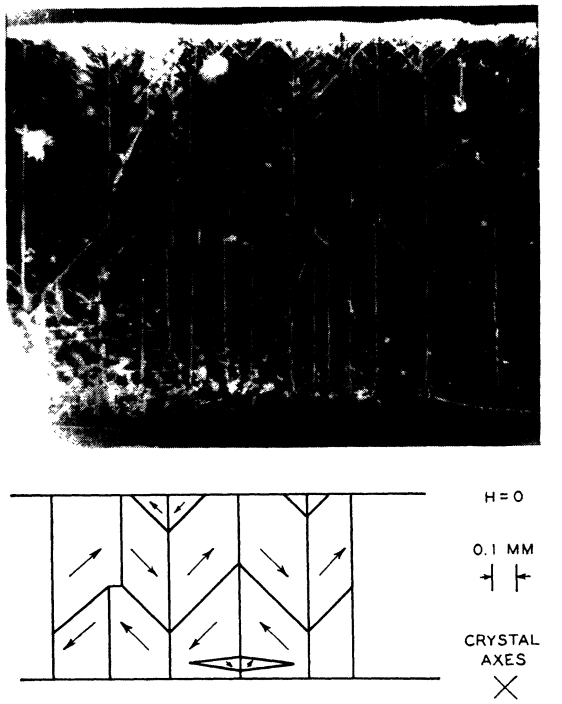


FIG. 27. Pattern on a (100) surface, and its interpretation.

edges. In addition it has, near the middle, some 180° boundaries inclined at 45° to the long dimension. Near the lower edge some tree-like patterns are formed. These have been previously commented on and are shown enlarged in Fig. 16.

Néel has related the distance between the lines of the pattern on the (100) surface, when the material as a whole is magnetized parallel to [0$\bar{1}$1] (Fig. 21 (d) to (g)), to the intensity of magnetization, when this is more than 0.7 of saturation. The theoretical prediction of decreasing distance with increasing magnetization is confirmed by our experiments, as well as by those of Kaya and of Sixtus. According to theory this distance, $W$, is independent of the thickness and length of the specimen and is calculable if one knows the intensity of magnetization and the width, $L$, of the specimens—in our experiment 0.20 cm. Néel has calculated $W$ for a specimen of iron having a width of 1 cm and an anisotropy constant, $K$, of 420,000, and has obtained a value of 50 microns for high magnetization ($\frac{3}{4}$ of saturation). In adapting this order-of-magnitude calculation to a crystal containing 3.8 percent silicon, the change in values of $K$ and $I_s$ can be disregarded. Using Néel's relation

$$W \propto (L)^{\frac{1}{2}},$$

it appears that $W$ should be about 20 microns for $B=15{,}000$. This is somewhat smaller than that observed, 100 microns, but it is close enough to suggest that the assumptions underlying the calculations are essentially correct.

A change of domain thickness with domain width has been observed near the corner of a crystal in which the domains are magnetized at 45° to the specimen edges, which are of the form ⟨110⟩. This is shown in Fig. 28.

Although this pattern is not understood in complete detail, certain general features appear sufficiently well established to permit a comparison between theory and experiment. The domains consist of long slabs magnetized parallel to the domain boundaries as indicated by the striations, the direction of magnetization alternating from slab to slab. Where the slabs meet the [110] edges, there must be small domains of closure, magnetized in part vertically where they meet the surface and in part horizontally at right angles to the main domains so as to close

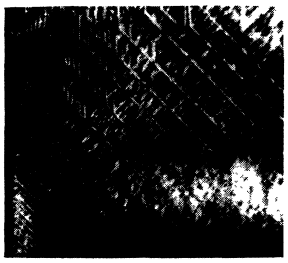


FIG. 28. Pattern on the corner of a crystal showing the increase in width of the domains as the length increases.

the flux pattern. Several possible domain structures have been devised to accomplish this closure using only easy directions and developing no poles; however, none of these has been verified directly from experiment. For all such patterns the closure domains extend inwards from the surface of the specimen to a depth roughly equal to the width $W$ of the domains. Since the closure domains are magnetized at right angles to the main domains, they have magnetostrictive energy "$s$," (see Section 6 in the Appendix), giving each domain a magnetostrictive energy of about $W^2s$ per unit depth. Each domain has a wall energy of $\gamma L$ per unit depth where $\gamma$ is the wall energy per unit area and $L$ the long dimension of the domain as seen in Fig. 29. Minimizing the total energy per unit volume of the specimen yields, in the usual way,[9,11,15] the result

$$W=(\gamma L/s)^{\frac{1}{2}},$$

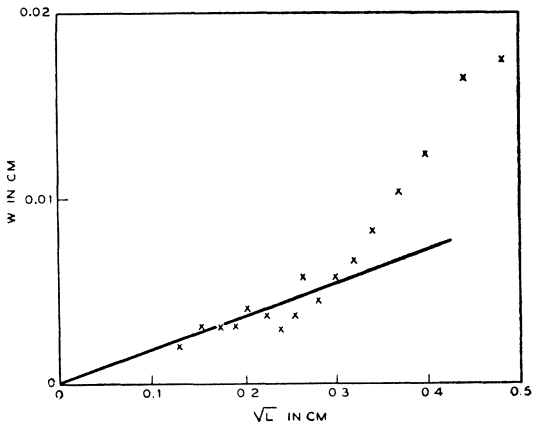


FIG. 29. Domain width as a function of the square root of the length for the pattern in Fig. 28.

[15] C. Kittel, Phys. Rev. **70**, 965 (1946).

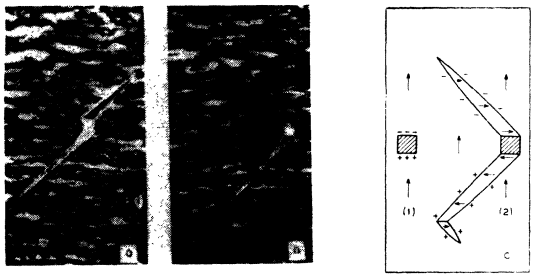


FIG. 30. Domain structure around holes in a crystal: (a) and (b), patterns observed; (c1) diagram showing a square hole with magnetic poles on opposite sides; (c2) diagram showing domains formed on opposite sides of a hole, as in (b), with consequent distribution of poles over tapered domains.

which is only approximate, since no detailed model of the domains of closure is employed. In order to test this relationship, values of $W$ have been plotted against $(L)^{\frac{1}{2}}$ as measured from Fig. 28. The straight line corresponds to $\gamma/s = 3\times10^{-4}$ cm which may be considered in fair agreement with $\gamma=1.5$ ergs/cm$^2$ and $s=10^3$ ergs/cm$^3$ in the absence of a detailed theory of the domains of closure. Large deviations from the straight line occur at $(L)^{\frac{1}{2}}$ greater than 0.35; at this point the measured domain pattern intersects another and deviations from the simple formula might be expected.

## DOMAIN STRUCTURE AROUND CAVITIES

Kersten's work[16] on the effect of cavities and nonmagnetic inclusions on the coercive force, and Néel's theoretical investigations[17] of the domain structure around them, prompted a search for powder patterns in such areas. Observation of a number of crystal surfaces under the microscope showed the presence of an occasional hole that had formed accidentally during the freezing or the etching or polishing of the crystal. The patterns around two holes in (100) surfaces are reproduced in Fig. 30. Careful examination of the character of the striations of colloidal particles indicates that the magnetization inside the long slender regions is oriented at 90° to that outside—that is, the lines are 90° boundaries. Many other patterns of similar form were observed.

[16] M. Kersten, Physik. Zeits. **44**, 63 (1943).
[17] L. Néel, Cahiers de Physique No. 25, 21 (1944).

Patterns of this type have been predicted by Néel on purely theoretical grounds and our patterns are a striking confirmation of his theory, which may be described as follows. Imagine a cubic or spherical hole in the middle of a domain, as indicated at (1) of Fig. 30(c). Then magnetic poles will exist on the surfaces normal to the direction of magnetization, and to these can be attributed a demagnetization energy,

$$E_0=(1/2)N_0I_s^2V_0.$$

$N_0$ is the demagnetizing factor, $V_0$ the volume of the hole, and $I_s$ the saturation intensity of magnetization of the material around the cavity. If domain boundaries are formed as at (2), poles will not be present at the edges of the cavity, but will be distributed along the domain boundaries as indicated by plus and minus signs. In this case there will be energy associated both with the demagnetization (a volume effect) and with the boundaries (an area effect):

$$E_d=NI_s^2V, \quad E_\sigma=\gamma A.$$

Here $N$ is the demagnetizing factor of the volume, $V$, enclosed by the domain boundaries and magnetized at right angles to the surrounding material, $\gamma$ is the energy per unit area of boundary, and $A$ the total area of the bounding surface or Bloch wall. According to theory, the size of the domain structure is defined by minimizing the sum of these two energies.

A rough calculation can easily be made of the size of domain to be expected around a hole of given size. Let the diameter of the hole (assumed spherical) be $d$, and let the shape of the domain be a rotational ellipsoid having minor axes $d$

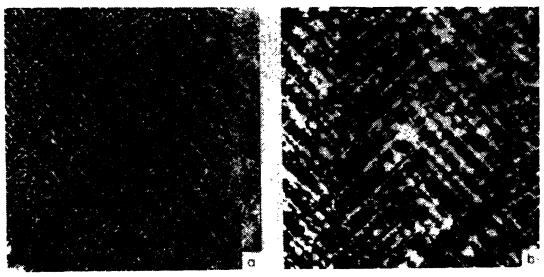


FIG. 31. (a) Pattern formed by air-blown carbonyl iron powder, after settling on a crystal; (b) pattern obtained by placing a drop of colloidal suspension on previously formed pattern of type (a).

and major axis $l$. When $l \gg d$, the demagnetizing factor of this ellipsoid is

$$N = 4\pi d^2[ln(2l/d) - 1]/l^2,$$

and the volume and surface are easily calculable. In estimating the magnetostatic energy, allowance should be made for the permeability of the domains themselves, resulting from the finite value of the anisotropy. This introduces a correction factor of about 1/25 as shown in Section 4 of the Appendix. Including this factor, the energies of the boundaries and the surface poles are

$$E_d = 16\pi^2 I_s^2 d^4[ln(2l/d) - 1]/75l,$$
$$E_\sigma = \pi^2 \gamma dl/4.$$

Using the numerical values $d = 0.001$ cm, $I_s = 1580$, $\gamma = 1.5$ ergs/cm$^2$, the value of $l$ for which $E_d + E_\sigma$ is a minimum is 0.10 cm and the ratio $l/d$ is approximately 100. The observed ratio of $l/d$ for the domain of Fig. 30(b) is about 50, smaller by a factor of two—satisfactory agreement in view of the simplifications employed.

### PATTERNS WITH DRY POWDER

Some patterns were formed by a different method. A fine grade of carbonyl iron powder, containing an appreciable number of particles less than 1$\mu$ in diameter, was placed under a bell jar and blown with a jet of high pressure air. This was allowed to settle for several minutes, the polished specimen was then placed under the bell jar and the finer particles allowed to settle on the specimen for several minutes more. The patterns so obtained are immobile and cannot be changed by changing magnetization or stress, and a separate pattern must be formed for each condition of the specimen. Figure 31(a) shows one pattern so obtained. In forming the pattern of Fig. 31(b) the powder was first allowed to settle as described and then colloidal solution was applied in the usual manner. The fine lines of colloidal magnetic particles are observed to coincide with the lines of coarser particles of carbonyl iron.

### PLASTIC DEFORMATION OF CRYSTAL

In studying the effect of tension on domain patterns of crystals of iron containing some silicon, it

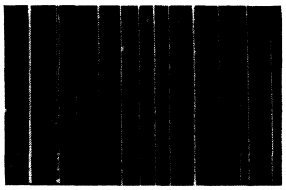


FIG. 32. Pattern on crystal of permalloy strained beyond elastic limit.

was observed that the original "tree" type of pattern for zero stress could be obtained repeatedly after removal of the stress as long as it was within the elastic limit.

An attempt was made to find a domain pattern, with or without tension, on a single crystal containing 76 percent nickel and the remainder iron. No distinct pattern could be observed until rather high stress was applied, whereupon a series of parallel lines appeared as indicated in Fig. 32. These remained after repeated magnetization and demagnetization, and even after electrolytic polishing and re-application of colloid, always in the same place in the crystal. Without the presence of colloid they could not be detected under the microscope. The specimen had been stretched in a [110] direction. The lines are parallel to [1$\bar{1}$0], in the surface parallel to (001). Observation over the edge of the specimen, on the (1$\bar{1}$0) plane, showed two sets of lines making angles of $\pm 55$ to 56° with the dege. There can be little doubt that the lines are caused by slip or incipient cleavage on (111) planes, for which the calculated angle is 54.7°.

This powder technique may be useful in observing plastic deformation or dislocations in the early stages, before their presence can be detected by other means.

We are indebted to Dr. C. Kittel for helpful discussions regarding domain theory, to Mr. J. G. Walker for valuable assistance with the photography and especially in the preparation of the specimens, and to Messrs. F. W. Ryan, R. A. Ehrhardt, and G. Bittrich for preparing the solution for electrolytic polishing and the ferromagnetic colloid.

## APPENDIX

### 1. Remarks

In this appendix we shall give an approximate treatment of the energies involved for surfaces almost parallel to (100). In all cases we shall suppose that the underlying domains are magnetized along the [010] and [0$\bar{1}$0] directions while the outward normal to the surface is parallel to the direction [0, sin$\theta$, cos$\theta$].

Several steps are necessary in evaluating the magnetostatic energy. When magnetic fields are present, the magnetization is deflected slightly from the easy directions in the underlying domains. This effect is taken account of in Section 2 by assigning an effective permeability tensor to the underlying domains. For each assumed pattern the distribution of magnetic poles is estimated (Section 3). In most cases this distribution consists of one part where the [010] and [0$\bar{1}$0] domains strike the surface of the specimen plus another part where superficial [100] and [$\bar{1}$00] domains, like the tree branches, join the underlying domains. This latter part does not lie on the surface of the specimen but on the curved domain wall. However, since the superficial domains on the surface are relatively shallow, it is assumed for purposes of calculation that the pole lies on the surface also and that the effect of the superficial domain that lies over it can be neglected. (A rough estimate indicates that this approximation may lead to overestimating the energy by about 25 percent.) Finally all the pole distributions considered are approximated by infinite parallel strips. The energies for three such cases are worked out in Section 4: here Case I corresponds to the underlying domain pattern with no superficial domains, II to the tree pattern, and III to the steep slope pattern for which the strips are narrow compared to their spacing.

The areas of the domain walls present a simpler problem and are estimated on the basis of hypotheses on the shapes of the domains.

It may be worth pointing out that the mathematical problems involved in predicting the shapes of domain walls from first principles are of very considerable difficulty. This arises from the fact that the energy of the wall per unit area depends on the direction of its normal; the poles on the wall surface depend on its normal and on the field arising from other walls and surface poles. In this treatment, shapes observed in experiment have been used as a guide; it can be seen on the basis of general principles that these shapes are reasonable. Energy estimates are then based on the observed shapes and the sizes are determined by minimizing the energy in Sections 5 and 6; this leads to a set of predicted dimensions for the domains which compare within a factor of 2 to 3 with those observed.

A list of the principal symbols used in the equations is as follows (constants refer to 3.8 weight percent silicon iron):

$I_s = 1580$ gauss (saturation magnetization),
$K = 280{,}000$ ergs/cm$^3$ (anistropy constant),
$\gamma = 1.5$ ergs/cm$^2$ (Bloch Wall Energy),†
$C_{11} = 2.37\times10^{12}$, $C_{12} = 1.41\times10^{12}$ ergs/cm$^3$ (elastic constants),
$h_1 = 3.2\times10^{-5}$ magnetostrictive strain (taken the same as for iron),
$\mu^*$ = effective permeability of a domain (see Section 2),
$\chi^*$ = effective susceptibility of a domain,
$s$ = magnetostrictive energy density (see Section 6),
$\psi$ = magnetostatic potential for finite $K$,
$\varphi$ = magnesostatic potential for infinite $K$,
$W$ = spacing between parallel strips in Cases I, II, III (see Section 4),
$S$ = width of strip (carrying poles) in Case III,
$a, b, c$ = dimensions in tree patterns (Fig. 12),
$e_1, e_2, e_3$ = magnetostatic energies in ergs/cm$^2$ of surface (Eqs. of Section 4),
$\theta$ = tilt of surface with respect to crystal axes,
$e_5$ = energy per unit area of tree patterns (Section 5),
$e_6$ = energy per unit area for steep slope patterns (Section 6),
$xyz$ = coordinates with respect to the surface of the specimen,
$XYZ$ = coordinates with respect to crystal axes.

### 2. The $\mu^*$ Method for Magnetostatic Energies

When the magnetization is nearly parallel to an easy direction, the dependence of magnetization, $I$, upon field strength, $H$, within a domain may be taken into account by assigning a permeability tensor $\mu^*$ which takes a diagonal form when the easy directions are chosen for the axes. Parallel to the easy direction nearest the direction

† This value is a rough average for several crystallographic directions, based on the formulae of L. Néel, Cahiers de phys. 25, 1 (1944), using the constants for iron

of magnetization, $\mu=1$ since the saturation magnetization is practically independent of the field. The magnetization will be rotated slightly for $H$ perpendicular to the easy direction, the equilibrium angle being given by minimizing the energy density

$$E=K[\alpha_2^2\alpha_3^2+\alpha_3^2\alpha_1^2+\alpha_1^2\alpha_2^2]-HI_s\alpha_1,$$

where $K$ is the anistropy constant, $\alpha_1$, $\alpha_2$, $\alpha_3$ are the direction cosines of the domain magnetization in respect to the $XYZ$ crystal axes, $I_s$ is the magnetization in the domain and $H$ the field, taken as parallel to the $X$ axis. If the domain is initially polarized parallel to $z$ (i.e., $\alpha_3=1$, $\alpha_1=\alpha_2=0$) and if its direction is specified by conventional polar angles $\theta$ and $\varphi$, we have for small angles

$$\alpha_1=\sin\theta\cos\varphi,\quad \alpha_2=\sin\theta\sin\varphi,\quad \alpha_3=\cos\theta,$$

$$E=K[\cos^2\theta\sin^2\theta+\sin^4\theta\sin^2\varphi\cos^2\varphi]-HI_s\sin\theta\cos\varphi$$
$$\doteq K\theta^2-HI_s\theta\cos\varphi,$$

giving a minimum for $\varphi=0$ and $\theta=HI_s/2K$. The corresponding magnetization is thus $I_x=HI_s^2/2K$, $I_y=0$, $I_z=I_s$. This leads (by symmetry) to the conclusion that the tensor $\mu$ is diagonal for axes $XYZ$ with components

$$\mu^*=1+4\pi I_s^2/2K$$

for $X$ and $Y$ and unity for $Z$. The values of $\mu^*$ and $\chi^*=I_s^2/2K$ for silicon iron are estimated as $\chi^2=(1580)^2/2\times280{,}000=4.5$ and $\mu^*=57$.

In order to discuss the energies in terms of $\mu^*$ and the surface poles, we introduce two sets of coordinates $XYZ$ in respect to the crystal axes and $xyz$ in respect to the surface of the specimen. We have

$$x=X,\quad y=Y\cos\theta-Z\sin\theta,$$
$$z=Y\sin\theta+Z\cos\theta.$$

The domains are assumed to be magnetized nearly parallel to the $\pm Y$ axis so that the axes of the permeability tensor $\mu$ are along $XYZ$ with values $\mu^*$, 1, $\mu^*$. However, for small angles $\theta$, no important error will be introduced by taking the axes of the $\mu^*$ tensor as along $x,y,z$.

An outline of the method of evaluating the magnetostatic plus anisotropy energy by the $\mu^*$ method†† is as follows (the mathematical details are given later): We first find the density of surface poles $\sigma_1(x,y)$ which would exist because of the tilt of the surface and the joining of superficial domains. Next we solve the magnetostatic problem which arises from placing $\sigma_1(x,y)$ on a block of material characterized by the $\mu^*$ tensor; this leads to a magnetostatic potential $\psi_1(x,y,z)$. Next we consider what internal magnetization $I$ would result from the field corresponding to $\psi_1(x,y,z)$ and how this would change the net surface pole density from $\sigma_1(x,y)$ to $\sigma_2(x,y)$ and also produce a volume pole density equal to $-\nabla\cdot I$. Finally, we verify that these poles on the surface and throughout the volume simply give $\psi_1(x,y,z)$ so that $\psi_1(x,y,z)$ is a self-consistent potential distribution. The total magnetostatic energy distribution can be calculated either from

$$E_M=\tfrac{1}{2}\int\sigma_1(x,y)\psi_1(x,y,0)dxdy$$

or by adding the stored anisotropy energy and $\int(H^2/8\pi)dxdydz$, the two giving identical results.

Proof: $\psi_1$ as derived from $\sigma_1$ must satisfy the equations

$$\nabla^2\psi_1=0,\qquad z>0,$$

$$\mu^*[(\partial^2\psi_1/\partial x^2)+(\partial^2\psi_1/\partial z^2)]+[\partial^2\psi_1/\partial y^2]=0,\qquad z<0,$$

$$\mu^*[(\partial\psi_1/\partial z)_{z=-0}]-[(\partial\psi_1/\partial z)_{z=+0}]=4\pi\sigma_1,\qquad z=0.$$

For all cases of interest, the total number of poles on the surface, i.e., $\int\sigma_1dxdy$, is equal to zero. Hence these equations determine uniquely a $\psi_1$ which vanishes at $z=\pm\infty$. Now this $\psi_1$ will alter the magnetization inside the underlying domains from $I_0=(0,\pm I_s\cos\theta,\pm I_s\sin\theta)$, which corresponds to $K=\infty$, by a vector amount

$$\delta I=[-\chi^*(\partial\psi_1/\partial x),\,0,\,-\chi^*(\partial\psi_1/\partial z)].$$

This gives rise to an internal volume pole of

$$-\nabla\cdot(I_0+\delta I)=-\nabla\cdot\delta I=+\chi^*[(\partial^2\psi_1/\partial x^2)+(\partial^2\psi_1/\partial z^2)],$$

since the domains corresponding to the $K=\infty$ distribution give $\nabla\cdot I_0=0$ and an added surface pole of

$$\sigma_3(x,y)=-\chi^*(\partial\psi_1/\partial z)=z\text{ component of }\delta I.$$

The net volume pole $-\nabla\cdot I$ and surface pole $\sigma_2=\sigma_1+\sigma_3$ now give rise to a magnetostatic

†† For earlier treatments of similar problems see references 9, 11, and 17.

potential $\psi_2$ which must satisfy

$$\nabla^2\psi_2 = -4\pi(-\nabla\cdot I) = -4\pi\chi^*[(\partial^2\psi_1/\partial x^2)+(\partial^2\psi_1/\partial z^2)]$$

and

$$[(\partial\psi_2/\partial z)_{z=-0}-(\partial\psi_2/\partial z)_{z=+0}] = 4\pi[\sigma_1-\chi^*(\partial\psi_1/\partial z)_{z=-0}].$$

It is readily verified by substitution that these equations are satisfied by letting $\psi_2$ equal $\psi_1$. In other words, $\psi_1$ is the self-consistent solution desired. In addition, it may be verified by letting $B=H+4\pi\delta I$ (in keeping with the $\sigma_1,\mu^*$ model) and noting that stored anisotropy energy is $\delta I^2/2\chi^*$, that the following three expressions for $E_M$ are equivalent:

$$E_M = \tfrac{1}{2}\int\sigma_1(x,y)\psi_1(x,y,0)dxdy$$

$$= \frac{1}{8\pi}\int H\cdot B dxdydz$$

$$= \int[(H^2/8\pi)+\delta I^2/2\chi^*]dxdydz.$$

We shall refer to this result as the $\mu^*$ method of calculating magnetostatic energies. It is obviously limited to cases for which $\theta$ and the deviations of magnetization from easy directions are all small.

### 3. Pole Density for $K=\infty$

When the magnetization is everywhere parallel to easy directions, the pole density on the surface or the domain walls is easily found. The density $\sigma_1$ on the surface of the [010] and [0$\bar{1}$0] domains is simply $\pm I_s\sin\theta$; this covers Case I and is one way of considering III.

For Case II, the tree patterns, the branches are [100] and [$\bar{1}$00] domains inserted in [010] and [0$\bar{1}$0] domains. The change in magnetization when [100] is inserted in [010] is equivalent to superimposing a new magnetization with components $I_s$, $-I_s$, 0. Thus, if the walls of the branches are parallel to [1$\bar{1}$0], no poles will be developed on the walls since they are parallel to the added magnetization; however, if they taper to a point, all of the flux entering the branch at the trunk eventually leaves through the wall. This is a particular example of a vector theorem relating to the poles appearing on the wall. If $n$ is the unit normal drawn from a domain with magnetization $I_1$ into a domain of magnetization $I_2$, then the net surface pole density is

$$\sigma = n\cdot(I_1-I_2).$$

Hence, if $n$ is perpendicular to $I_1-I_2$, i.e., if $I_1-I_2$ lies in the plane of the wall, the pole density is zero. For the case of the tree patterns the branches represent strips of varying width, having varying pole density cutting across a sky of uniform pole density (Fig. 13). This is approximated in Case II, treated below, by a pattern of strips of uniform pole density of equal width and alternating sign cutting at 45° across the specimen. This approximation tends to underestimate the actual energy and thus offsets the effect of neglecting the material in the branches lying above the wall surface as discussed in the introduction to the appendix.

### 4. Magnetostatic Energies for Special Cases

*Case I*

As shown in Fig. 11, the domains of width $W$ are polarized approximately along $\pm Y$ so that the pole density for $K=\infty$ is $\sigma=\pm I_s\sin\theta$. For this structure, $\psi_1$ cannot depend on $y$ so that the field $H$ lies in the $xz$ plane, in which the domains have permeability $\mu^*$. Hence the potential $\psi$ (omitting the subscript "1") needed in the expression for $E_M$ (Section 2) must satisfy

$$\nabla^2\psi(x,z)=0,$$

$$+\frac{\mu^*\partial\psi}{\partial z}\Big]_{z=-0} - \frac{\partial\psi}{\partial z}\Big]_{z=+0} = 4\pi\sigma(x).$$

This solution is simply related to $\varphi(x,z)$, the solution of the simpler problem for $\mu^*=1$. It is readily verified that if $\varphi(x,z)$ is known, then the desired solution is

$$\psi(x,z)=2\varphi(x,z)/(1+\mu^*).$$

The energy $E_M$ is then

$$E_M = \frac{2}{1+\mu^*}\int\varphi(x,0)\sigma(x)dxdy.$$

The integral has been evaluated by expanding $\varphi(x,z)$ in a series, $\exp[(n\pi/W)(\pm z\pm ix)]$, this

leading to

$$e_1 = 1.70 I_s^2 (\sin^2\theta) W/(1+\mu^*)$$

for the average energy per unit area, which in the limit $\mu^* = 1$ agrees with a result obtained by Kittel.[15]

*Case II*

For the case of the tree patterns we estimate the magnetostatic energy by replacing the branches and sky by parallel strips, each of width $W$ having pole density $I_s \sin\theta$ running at 45° to $x$ and $y$ on the surface. For this case the surface pole density and potential may be taken to be $\sigma(x+y)$ and $\varphi(x+y,z)$ for $K = \infty$. For finite $K$ we try the solution

$$\psi(x+y,z) = A\varphi(x+y,z), \quad z>0,$$
$$\psi(x+y,z) = A\varphi(x+y,az), \quad z<0.$$

The constant "$a$" is evaluated from $\nabla \cdot B = 0$ which gives

$$\mu^*(\partial^2\psi/\partial x^2) + (\partial^2\psi/\partial y^2) + \mu^*(\partial^2\psi/\partial z^2)$$
$$= (1+\mu^*)A(\partial^2\varphi/\partial x^2) + \mu^* a^2 A(\partial^2\varphi/\partial z^2) = 0,$$
$$a = ((1+\mu^*)/2\mu^*)^{\frac{1}{2}},$$

since $\nabla^2\varphi = 0$. $A$ is then evaluated from the condition of surface poles and is found to be

$$A = 2/(1+(\mu^*(1+\mu^*)/2)^{\frac{1}{2}}) = 2/(1+40.7) = 1/20.8,$$

so that the energy per unit area of surface in this case

$$e_2 = 1.70 I_s^2 (\sin^2\theta) W/(1+(\mu^*(1+\mu^*)/2))^{\frac{1}{2}}.$$

*Case III*

For the case of patterns on steeply sloping surfaces, we shall initially neglect the jagged edges of the patterns and consider strips of uniform pole density $\sigma$ and width $S$ spaced with period $W$ (when $S = W$ we have Case I). This case may be calculated by Fourier series or by an approximate method. According to the approximate method, we calculate $\varphi$ at the center of one strip (at the origin of $x$ and $z$) assuming that all the other strips are infinitely narrow. Taking the additive constant in the potential so that two unit lines of poles have potential $-2\ln r$, the potential at one strip due to all the others may be evaluated from

$$-2Re(\ln \tan\pi(x+iz)/2W) + 2\ln r.$$

This gives $-2\ln\pi/2W$ for the potential at the origin. The self-energy of the strip of unit pole density and width $S$ at the origin is

$$(1/2S^2)\int_0^S\int_0^S -2\ln|x-y|\,dxdy = \tfrac{3}{2} - \ln S.$$

To get the total self-energy per strip, to its own self-energy we add one-half its energy of interaction with all the other strips and obtain

$$\tfrac{3}{2} - \ln S + \tfrac{1}{2}(-2\ln\pi/2W) = \tfrac{3}{2} + \ln 2W/\pi S.$$

For the case under consideration, the pole density on each strip is not unity but $SI_s\sin\theta$ and the length of strip per unit area is $1/W$ so the total energy per unit area is

$$e_3 = (3+2\ln 2W/\pi S)S^2 I_s^2(\sin^2\theta)/W(1+\mu^*).$$

This expression should be quite accurate for $W \gg S$. As $S$ approaches $W$ an appreciable error will occur because the interaction between adjoining strips will differ from $+2\ln W$. However, even when $W = S$ the error is not great and the equation gives 2.16 instead of 1.70 for the numerical factor. (Introducing the correct energy for nearest neighbors reduces the error to less than 1 percent.)

## 5. Size Estimates for Patterns on Sloping Surface

In order to check the theory against experiment, a series of patterns was photographed on a uniformly curving surface varying in slope from $\theta = -5°$ to $\theta = +5°$. The patterns observed, which were similar to those of Fig. 10 but not as good photographically, could be classified as follows:

Simple parallel slabs: less than 0.5°; no branches.
Transition: 0.5° to 0.65°; trees form and branches grow to about $W/2$ in length.
Tree patterns: 0.65° to 1.30°; branches fill more of pattern finally eliminating trunk of tree.
Transition: 1.30° to 1.9°; branches begin to squeeze out sky.
Steep slope patterns: 1.9° to 3.9°; branches, cover all but a narrow strip of sky.

Except for the transition regions, it is possible to make rough estimates for the minimum energy configurations and check the dimensions with those obtained experimentally. The width $W$ of the underlying domains is determined by the

TABLE I. Comparison of measured and calculated dimensions of tree pattern (Fig. 12).

| | | | | | |
|---|---|---|---|---|---|
| Measured | | | | | |
| $\theta$ (degrees) | 1.0 | 1.3 | 2.0 | 2.6 | 3.2 |
| $a$ (mm) | 0.071 | 0.067 | | | |
| $b$ (mm) | 0.067 | 0.067 | | | |
| $S$ (mm) | | | 0.025 | 0.14 | 0.08 |
| Computed | | | | | |
| $c/b$ | 0.05 | 0.07 | | | |
| $a$ (mm) | 0.197 | 0.152 | | | |
| $b$ (mm) | 0.115 | 0.115 | | | |
| $S$ (mm) | | | 0.73 | 0.43 | 0.28 |

overall dimensions of the specimen and is considered a specified quantity. The dimensions measured for several angles are given in Table I. The quantities $a$, $b$, $c$ are defined in Figs. 21 and 13 and $S$ in Fig. 14. The value of $W$ is 0.6 mm throughout.

In treating the tree patterns we assume that the branches of the trees nearly neutralize the net flux. This is reasonable since lack of neutralization is much more important for the wide strips between trunks ($W \doteq 0.2$ mm) compared to the branch width and spacing ($W \doteq 0.02$ mm). Starting with this assumption and assuming, furthermore, that the branches are elliptical cones, as indicated in Fig. 12, it is possible to determine the ratio of depth $c$ to width $b$ from the experimental data as follows. The flux carried by one branch is $I_s \pi bc/2$. Each branch neutralizes an area of $aW/2$ with pole density $I_s \sin\theta$. This gives

$$I_s \pi bc/2 = aWI_s(\sin\theta)/2,$$
$$c/b = aW(\sin\theta)/\pi b^2.$$

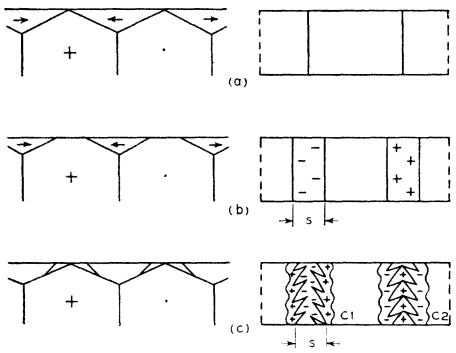


FIG. 33. Closure patterns for steeply sloping surface: (a) complete closure, (b) pattern with strips of alternating sign, (c) pattern with strip with no net pole density.

From these, the values of $c/b$ have been computed and are tabulated in Table I. These indicate that taking $c/b$ as 1/20 will be a satisfactory approximation. This gives

$$b = (20aW(\sin\theta)/\pi)^{\frac{1}{2}}.$$

We next start with the estimated values for $\theta$, $W$ and $c/b$ and try to calculate $a$ and $b$ by minimizing the energy. The magnetostatic energy is estimated from Case II taking $W = a/2\sqrt{2}$; this introduces $\sqrt{8}$ into the denominator in $e_4$ (see below). Replacing the branch and sky pattern by parallel strips of equal width is obviously a crude approximation; also Case II corresponds to strips all lying in the $xy$ plane, whereas the poles on the branches lie below the plane and are actually underneath permeable material. For these reasons we should regard the use of $e_2$ as being only a first approximation to the correct magnetostatic energy. If the cones were infinitely thin ($c/b = 0$) and the sides were straight, then the domain wall surface per unit area of the $xy$ plane would be $b/2a$. Actually the branches have depth and are also slightly bulged, this increases the fraction; on the other hand they do not run to the center. We therefore compromise by using domain wall area per unit surface areas equal to

$$b/2a = (20W(\sin\theta)/4\pi a)^{\frac{1}{2}}.$$

The total energy for this case is, therefore,

$$e_4 = \frac{1.70aI_s^2 \sin^2\theta}{(1+(\mu^*(1+\mu^2)/2))^{\frac{1}{2}}(8)^{\frac{1}{2}}} + \gamma[20W(\sin\theta)/4\pi a]^{\frac{1}{2}}$$
$$= Aa \sin^2\theta + B(W \sin\theta/a)^{\frac{1}{2}},$$

where

$$A = \frac{1.70I_s^2}{(1+(\mu^*(1+\mu^*)/2)^{\frac{1}{2}}(8)^{\frac{1}{2}}} = \frac{1.70(1580)^2}{(41.7)(2.83)} = 3.60\times10^4,$$

$$B = \gamma(20/4\pi)^{\frac{1}{2}} = 1.5(5/\pi)^{\frac{1}{2}} = 1.89,$$

the units being c.g.s. The value of $a$ which gives the least energy is readily found to be

$$a = (B/2A)^{\frac{2}{3}}W^{\frac{1}{3}}/\sin\theta = 8.83\times10^{-4}\times(0.06)^{\frac{1}{3}}/\sin\theta = 3.45\times10^{-4}/\sin\theta$$

from which the computed values of $a$ in Table I are obtained. Combining these with the formula $b=(20aW)[(\sin\theta)/\pi]^{\frac{1}{2}}=1.15\times10^{-2}$ cm gives the value for $b$. The agreement between observation and calculation is fair, the calculated $a$ and $b$ being about 2.5 and 1.7 times the observed. The value for $a$ depends upon $(b/c)^{\frac{1}{2}}$ power and is, therefore, insensitive to the assumed value. However, the agreement indicates the essential correctness of the physical picture.

The total energy per unit area is

$$e_5=\tfrac{3}{2}(2AB^2)^{\frac{1}{3}}W^{\frac{1}{3}}\sin\theta.$$

This formula should be fairly good for the range in which $b\cong a/2$, say from $b=a$ to $b=a/3$, corresponding to $\theta=0.6$ to $1.7°$.

### 6. Size Estimates for Steeper Slopes

Two models of the domain structure beneath the surface have been investigated. These are illustrated in Fig. 33: (a) represents the flux closure case, (b) shows the case discussed above for which there is a net pole density at the center of each [010] domain surface, (c) has no net pole density (since the transverse domains are deep enough to carry the required flux from each [010] to $[0\bar{1}0]$ domain as in (a)); however, the walls have been pulled back to produce the type of pattern shown.

Calculations based on model (b) (but omitted from this appendix) lead to strip width 10 to 20 times narrower than observed, the reason being that the magnetostatic energy (see Section 4) of widely separated strips, on which lie poles, is high. Model (c) leads to widths about one third of the experimental values. On the basis of the interpretation of (c), the energy will be less for the staggered distribution $c_1$ than for $c_2$, since the former tends to move like poles farther apart; this is in agreement with the appearance of the patterns of Fig. 10(d), (e), and (f).

For slopes of 3° and widths of $W=0.6$ mm, the magnetostrictive energy in the transverse domains is comparable to the wall energy. The transversely magnetized domains are forced to fit the large underlying domains. This means the transverse domain is strained out of its equilibrium (i.e., zero stress) shape of strains of $\epsilon_{xx}=-\epsilon_{yy}=-h_1$, $\epsilon_{zz}=\epsilon_{xy}=\epsilon_{yz}=\epsilon_{xz}=0$, where $h_1$ is the fractional increase in length in the $X$ direction in an unstressed domain when the magnetization is rotated from $Y$ to $X$.[18] The energy density is thus

$$\tfrac{1}{2}c_{11}(\epsilon_{xx}^2+\epsilon_{yy}^2)+c_{12}\epsilon_{xx}\epsilon_{yy}=(c_{11}-c_{12})h_1^2.$$

The values of these constants for iron are[19]

$$c_{11}=2.37\times10^{12},\quad c_{12}=1.41\times10^{12}\ \text{ergs/cm}^3,$$
$$h_1=3.2\times10^{-5}$$

giving a magnetostrictive energy density of

$$s=0.96\times10^{12}\times(3.2)^2\times10^{-10}=0.98\times10^3\ \text{ergs/cm}^3.$$

The volume having this energy is $\sin\theta(W-S)^2/4$ per unit length along $y$ and width $W$, hence the energy per unit area of surface is

$$s\sin\theta(W-S)^2/4W.$$

For $\theta=3°$ and $W=0.6$ mm this gives 0.75 erg/cm² which is comparable with the wall energy of about 1.5 ergs/cm².

In model (c), we treat each strip $S$ as a pattern of alternating strips at 45°. This leads to using Case II with $W_2=S/4$ as an estimate from the pattern of Fig. 10 (f). A fraction $S/W$ of the surface is covered with the strips. The reduction of wall surface per unit length of strips is about $1/2S$ based on the projected area and is perhaps $0.3S$ considering the fact that the wall boundary is curved. The average energy per unit area is

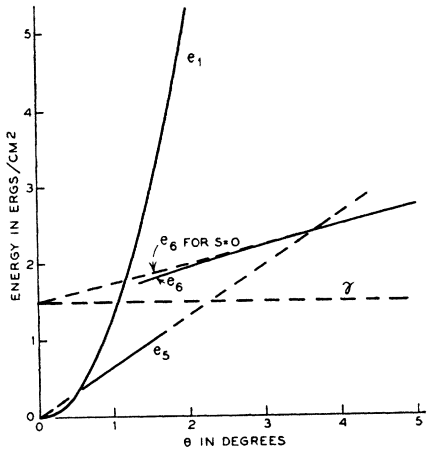


FIG. 34. Comparison of energies for simple parallel slabs ($e_1$), tree patterns ($e_5$), and various approximations for steep slope patterns ($\gamma$, $e_6(S=0)$, $e_6$).

[18] F. Bitter, *Introduction to Ferromagnetism* (McGraw-Hill Book Company, Inc., New York, 1937), p. 248.
[19] Reference 18, p. 254.

thus

$$e_6 = s(\sin\theta)W/4 + \gamma(1 - 0.3S/W) + 1.70S^2I_s^2(\sin^2\theta)/4W(1+(\mu^*(1+\mu^*)/2))^{\frac{1}{2}}.$$

This leads to a minimum energy for

$$S_{\min} = 0.3\gamma/[1.70I_s^2/2(1+(\mu^*(1+\mu^*)/2))^{\frac{1}{2}}]\ \sin^2\theta = 0.3\gamma/\sqrt{2}A\ \sin^2\theta,$$

where $A = 3.60\times10^4$ as defined in Section 5. The energy is then

$$e_6 = s(\sin\theta)W/4 + \gamma(1 - 0.15S_{\min}/W)$$

(neglecting the small correction to the magnetostatic energy). Values of $S_{\min}$ so calculated are given in Table I and are about 3 times the measured values.

### 7. Comparison of Total Energies

In Fig. 34, the three energy expressions are plotted as functions of $\theta$. The $e_1$ curve is valid over the range of validity of the $\mu^*$ method; since the latter is limited by the condition that $\theta$ is small, this curve is certainly accurate to $\theta > 2°$. The $e_5$ approximation, however, depends on having $b \cong a/2$; the range of $b=a$ to $b=a/3$ is shown as heavy and represents an extension of $e_5$ somewhat beyond its range of validity. Three approximations to the steep slope patterns are shown: $\gamma$ corresponds to placing $S=0$ and neglecting magnetostriction; $e_6$ for $S=0$ adds the effect of magnetostriction; $e_6$ shows the best approximation with $S=S_{\min}$. Figure 34 is seen to explain the general trend of one type of pattern to another satisfactorily, the incidence of tree patterns at $\theta \cong 0.5°$ being given correctly. The weakest feature is the $e_5$ curve which has not been treated accurately enough to give properly the transition from tree to steep slope patterns.

PHYSICAL REVIEW VOLUME 75, NUMBER 1 JANUARY 1, 1949

# A Simple Domain Structure in an Iron Crystal Showing a Direct Correlation with the Magnetization

H. J. WILLIAMS AND W. SHOCKLEY
*Bell Telephone Laboratories, Murray Hill, New Jersey*

(Received August 30, 1948)

A hollow rectangle cut from a single crystal of 3.8 percent silicon iron has been studied with the aid of powder patterns and flux measurements. The edges and surfaces were all cut accurately parallel to ⟨100⟩, the directions of easy magnetization. The domain pattern consists of 8 domains, four forming an inner rectangle magnetized in one direction and the others forming an oppositely magnetized outer rectangle. Changes in magnetization occur by the growth of one set of domains at the expense of the other. In the saturated condition, each leg of the rectangle is one domain about $1.5\times0.1\times0.1$ cm in size. Implications of these results in connection with Barkhausen effect are discussed, and a method of measuring the energy of the Bloch wall is proposed.

THE theory of magnetic domains has been developed over a period of years to explain the gross magnetic properties of matter in terms of the behavior of smaller regions of substantially uniform magnetization. However, except for certain artificially simplified cases such as fine stressed wires or very small particles, it has not been possible to obtain a complete picture of the domain structure in any actual specimen and to show how it explains the state of magnetization and variations thereof. The experiments described below furnish an example of correlation between domain structure and magnetization for a specimen having a dimension of the order of one centimeter.

This specimen was in the form of a hollow rectangle (or "picture frame") of 3.8 weight percent silicon iron cut from a single crystal so as to have all edges and surfaces substantially parallel to [100] or equivalent directions. It had origi-

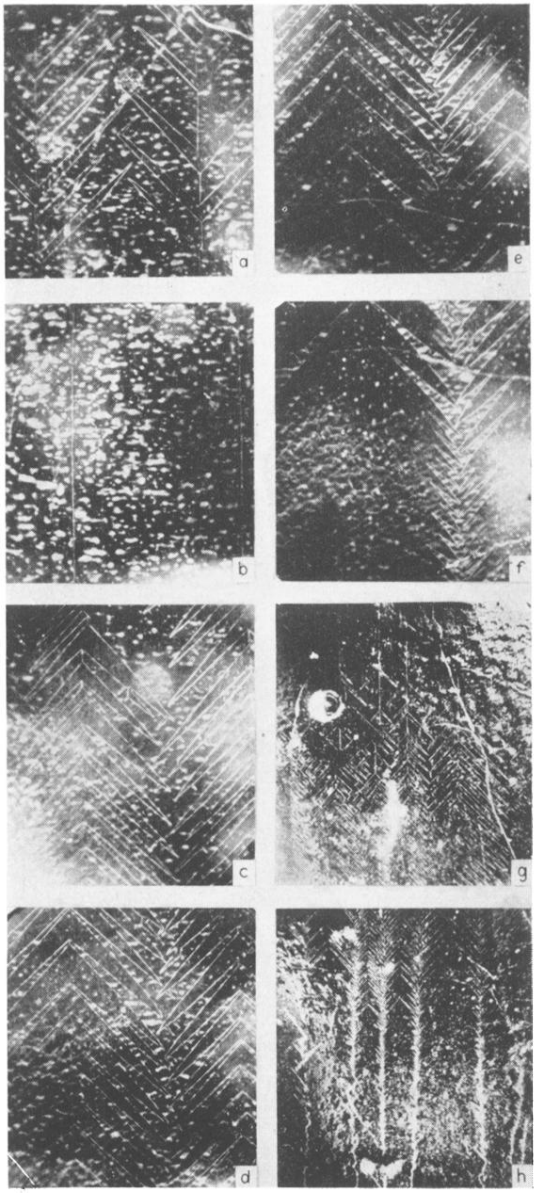


FIG. 10. Series of patterns observed at successive positions, (a) to (f), on a curved surface. Note correspondence to Fig. 9. Patterns in (g) and (h) were obtained with lower magnification, on surfaces corresponding to (b) to (d) and (d) to (f), respectively.

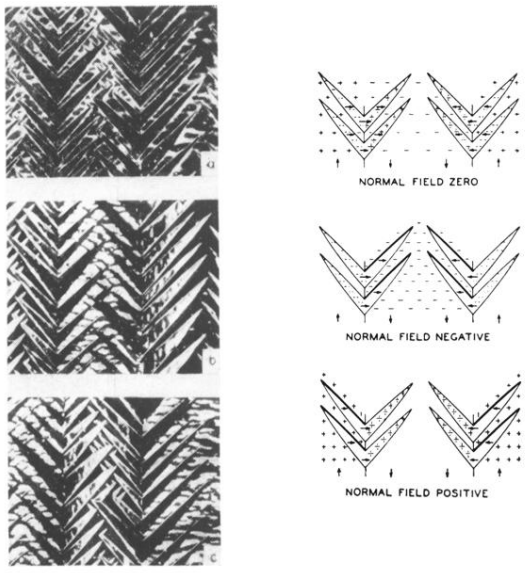


FIG. 15. Tree patterns showing the effect of applying a field of 30 Oersteds normal to the surface; (a) normal field zero, (b) normal field directed into the surface, (c) normal field directed outward from the surface.

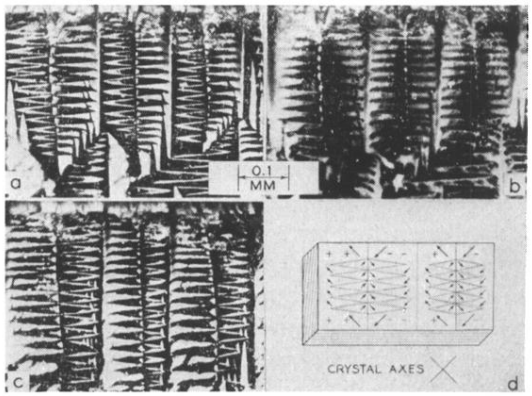


FIG. 16. Second kind of tree pattern; (a) field applied normal to the surface, (b) normal field zero, (c) normal field reversed, (d) diagram of directions of magnetization in the domains, crystal axes, and the inclination of the surface to the atomic planes (represented by lines on crystal edges).


FIG. 18. Tree pattern with field applied normal to the surface, showing redistribution of colloid over the domains, intensification of some domain boundaries and disappearance of others, as compared with pattern obtained with no normal field (cf. Fig. 15).

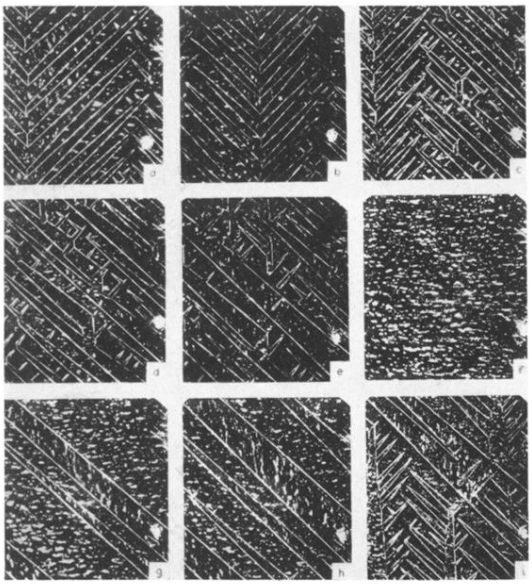


FIG. 19. Patterns on a surface inclined slightly to a (100) plane, with applied field and length of the crystal parallel to the [001] direction: (a) $B=0$, (b) $B=7000$, (c) $B=10{,}000$, (d) $B=11{,}600$, (e) $B=15{,}000$, (f) $B=18{,}600$, (g) $B=17{,}600$, (h) $B=17{,}400$, (i) $B=15{,}400$.

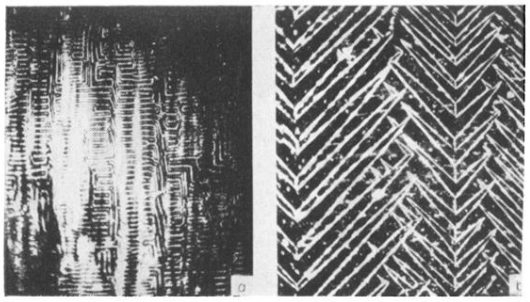

Mechanical polishing Electrolytic polishing

Crystal axes + →|0.1 mm|←

FIG. 2. Powder patterns obtained after mechanical polishing (a) and after electrolytic polishing (b) of the same surface area.

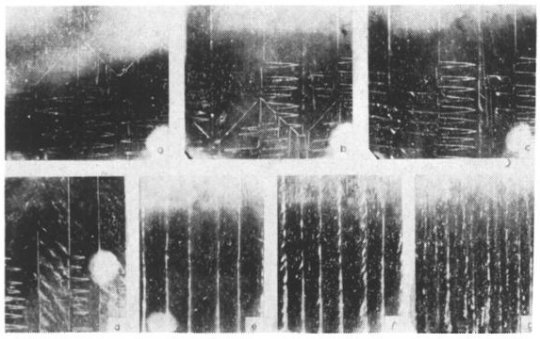


FIG. 21. Patterns on a (100) surface, with length of crystal and applied field parallel to the [011] direction. (a) $B=0$, (b) $B=9000$, (c) $B=14{,}500$, (d) $B=15{,}500$, (e) $B=15{,}900$, (f) $B=18{,}500$, (g) $B=20{,}000$.

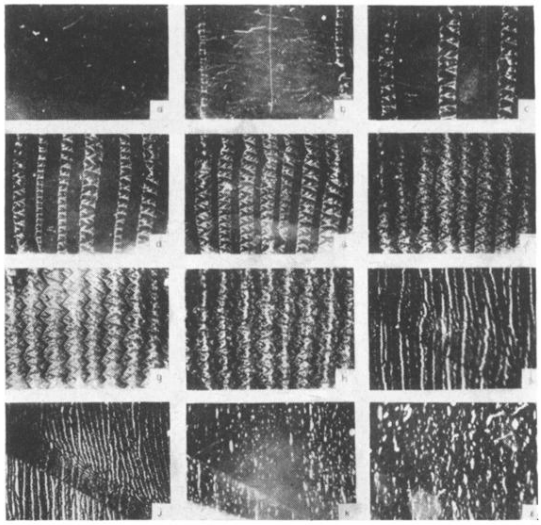


FIG. 22. Patterns on a (110) surface, with length of crystal and applied field parallel to the [1$\bar{1}$0] direction. (a) $B=0$, (b) $B=14{,}800$, (c) $B=15{,}000$, (d) $B=15{,}200$, (e) $B=15{,}700$, (f) $B=16{,}400$, (g) $B=17{,}100$, (h) $B=18{,}200$, (i) $B=20{,}000$, (j) $B=20{,}200$, (k) $B=20{,}300$, (l) $B=20{,}500$.

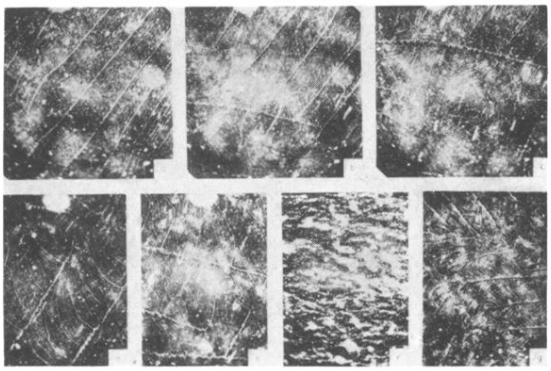


FIG. 23. Patterns on a (111) surface. (a) $B=0$, (b) $B=4000$, (c) $B=4800$, (d) $B=15{,}000$, (e) $B=15{,}500$, (f) $B=19{,}800$, (g) pattern on another area ($B=0$).

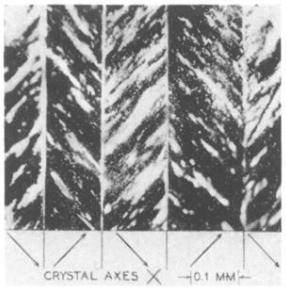


FIG. 25. Pattern obtained with a concentrated colloid on a (110) surface with striations of colloid indicating directions of magnetization (perpendicular to striations).

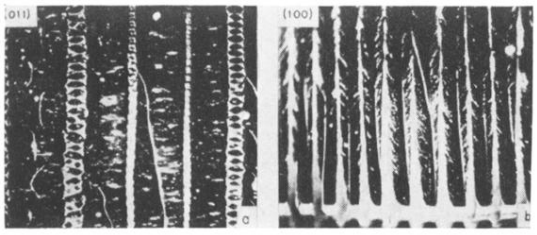


FIG. 26. Patterns obtained on the side and top surfaces of a crystal such as that shown by the drawing of Fig. 24: (a), (011) surface; (b), (100) surface. The lower part of the (b) pattern shows accumulations of colloid extending beyond the edge of the crystal.

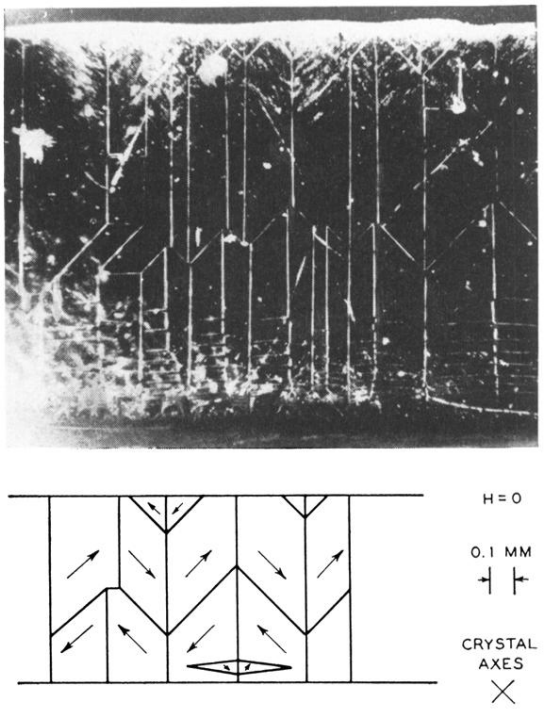


FIG. 27. Pattern on a (100) surface, and its interpretation.

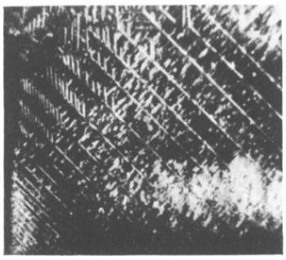


FIG. 28. Pattern on the corner of a crystal showing the increase in width of the domains as the length increases.

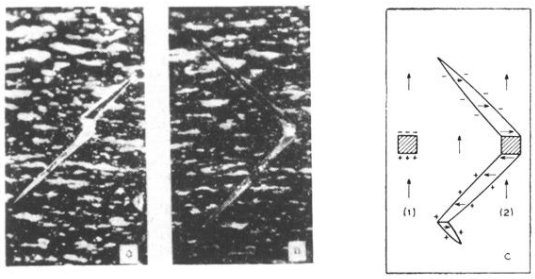


FIG. 30. Domain structure around holes in a crystal: (a) and (b), patterns observed; (c1) diagram showing a square hole with magnetic poles on opposite sides; (c2) diagram showing domains formed on opposite sides of a hole, as in (b), with consequent distribution of poles over tapered domains.

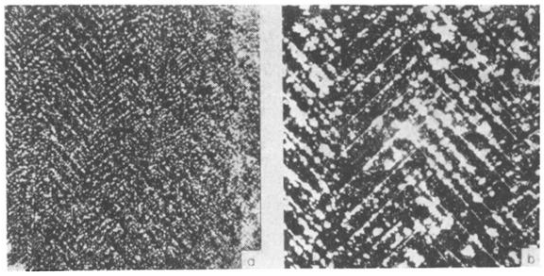


FIG. 31. (a) Pattern formed by air-blown carbonyl iron powder, after settling on a crystal; (b) pattern obtained by placing a drop of colloidal suspension on previously formed pattern of type (a).

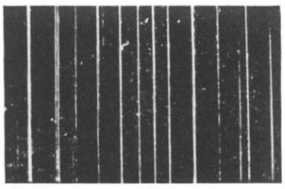

Permalloy, 76 percent nickel
Crystal axes ×  |← 0.1 mm →|
Tension ⟷

FIG. 32. Pattern on crystal of permalloy strained beyond elastic limit.

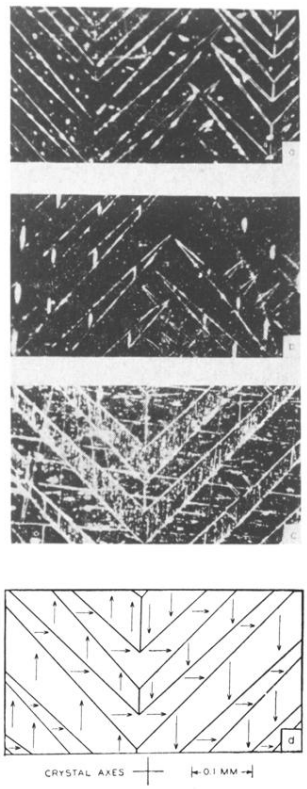


FIG. 4. (a) Typical "tree" pattern; (b) pattern on a surface having a series of parallel scratches made with a ruling engine; (c) pattern on a surface having vertical and horizontal scratches made with a brush of fine glass fibers; (d) directions of magnetization in pattern (c), as determined by the scratches.

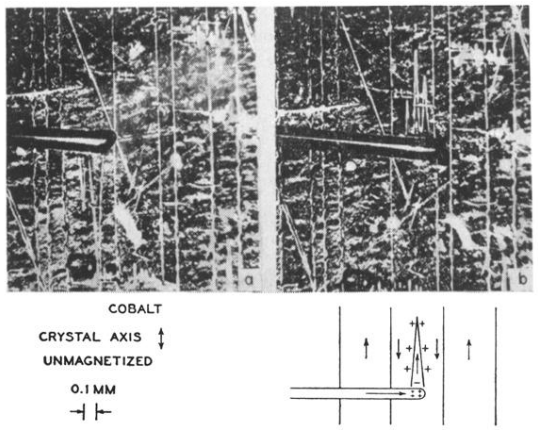


FIG. 5. Powder pattern showing regions of reversed magnetization induced by a permanent magnet probe, (a) before and (b) after moving the probe to the right so that it is above the adjacent domain. In (b) the regions of reversed magnetization are above the probe, in (a) they are below.

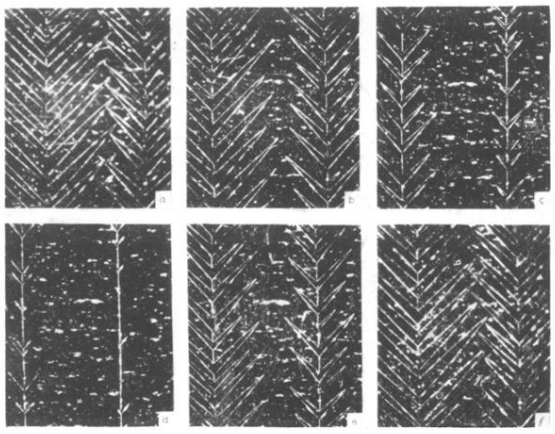


FIG. 6. (a) to (d), patterns all observed on the same area of a crystal, with tension increasing from zero to a maximum value. In (d) to (f) tension is decreasing from maximum value to zero.

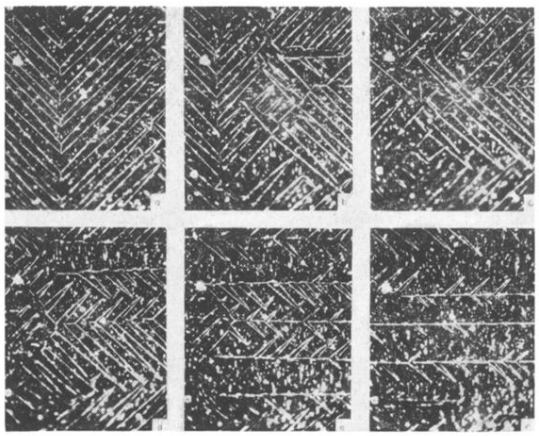


FIG. 7. Series of patterns, all observed on the same area of a crystal, as the compression was increased from zero to a maximum value.

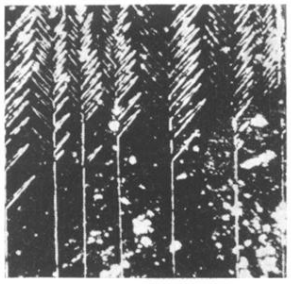


FIG. 8. Powder pattern on a surface having the lower half accurately parallel to a (100) plane, and the upper half inclined at an angle of 3° by rotation about a horizontal axis at the intersection of the two surfaces.